2010-01-01

Microstructure And Property Evaluation Of LiFePO4 Thin Films For Application In Microbatteries

Jose Marcos Mares
University of Texas at El Paso, jmmares@miners.utep.edu

MICROSTRUCTURE AND PROPERTY EVALUATION OF $LiFePO_4$ THIN FILMS FOR APPLICATION IN MICROBATTERIES

JOSE MARCOS MARES

Department of Mechanical Engineering

APPROVED:

_____
Ramana V. Chintalapalle, Ph.D., Chair

_____
Arturo Bronson, Ph. D.

_____
Jose Espiritu, Ph. D.

_____
Patricia D. Witherspoon, Ph. D.
Dean of the Graduate School

Dedicated to my Parents

MICROSTRUCTURE AND PROPERTY EVALUATION OF $LiFePO_4$ THIN FILMS FOR APPLICATION IN MICROBATTERIES

by

JOSE MARCOS MARES

THESIS

Presented to the Faculty of the Graduate School of

The University of Texas at El Paso

in Partial Fulfillment

of the Requirements

for the Degree of

MASTER OF SCIENCE

Department of Mechanical Engineering

THE UNIVERSITY OF TEXAS AT EL PASO

December 2010

Acknowledgments

First of all, I would like to express my deepest gratitude to Dr. C. V. Ramana. I thank him not only for his guidance on this project but also for his care for me in all this time. I will never forget his patience, accessibility, and guidance. His confidence in me always encourages me to do better. Whenever I look back the years passed, I always feel myself fortunate enough to have chosen him as my adviser.

I wish to express my sincere appreciation to Dr. Jose Espiritu, and Dr. Arturo Bronson for being in my committee and review my thesis work.

I would also like to thank all my research team members Satya Gullapalli, Rama Verumi, Guillermo Carbajal, and Narasimha Raju for their help and encouragement. My special thanks shall go to Dr. Kamala Bharathi for his assistance and guidance in all the experiment for this thesis work.

Finally, I would like to express my best thanks to my family and friends. I especially want to thank my parents. Without their selflessness, love and support, I may not be able to earn this degree.

Abstract

The shortage of fossil fuels and the requirements to produce clean, environmental friendly, efficient, and economical energy are the principal problems in the context of energy technology for current and future generations. Therefore, advanced energy storage and conversion capabilities with higher capacity and efficiency are desired. Currently, there is an enormous interest in the development of high energy density rechargeable batteries for use in domestic applications, automotive industries and portable electronic applications. The present research focuses on the development of $LiFePO_4$ thin films for solid-state thin-film microbatteries. The present effort was performed with a specific purpose of understanding the effect of temperature, an important thermodynamic variable, on the microstructure and electronic properties of $LiFePO_4$ films fabricated by radio-frequency (RF) magnetron sputtering. $LiFePO_4$ films were grown under varying deposition temperatures in the range of 25 to 400 °C. In addition, $LiFePO_4$ films were annealed in temperature ranges of 400 to 800 °C for 1 and 2 hours. The effect of growth temperature on the crystal structure, surface morphology, chemical quality and electronic properties is investigated in detail. Characterizations of the films were performed using X-ray diffraction (XRD), high resolution scanning electron microscopy (HRSEM), energy dispersive X-ray spectrometry (EDS), optical spectrophotometer, and electrical resistivity measurements. The grain size increased as the annealing temperature increased from 400 to 800 °C. The optical properties of the $LiFePO_4$ films indicate that, as the growth temperature is increased, the transmittance of the films increases.

The band gap increases from 2.75 eV to 3.28 eV with increasing temperature from RT-400 °C. When the films were annealing at 1 hour form 400-800 °C, the band gap increased from 3.12 eV to 3.7 eV. Annealing for 2 hours at temperatures from 400 to 800 °C showed an increase

in band gap 3.12 eV to 3.75 eV showing the maximum value at 600 °C. The electrical capacity indicates that with an increase in substrate temperature, the resistivity of the films also increases.

Table of Contents

List of Tables

List of Figures

Chapter 1: Introduction

Nowadays, there is a scarcity of fossil fuels and environmental concerns across the globe. It is now convinced that the green energy and related industries will become the main stream in the next years to resolve these critical problems. Therefore, there is an immense interest in the development of new energy storage systems with enhanced efficiency and can achieve the best possible energy density. Currently, there is a strong demand of high density rechargeable batteries.

The demand for high energy density rechargeable batteries has been increasing in the previous years and it will increase more in the next years due to portable electronics devices, energy storage systems and new technology. In addition, there will be an urgent need for more automobiles due to world population growth and this is one of the most important issues for the next generations. It is expected that there will be 1.6 billion automobiles in the year 2025 and the total emission of CO_2 will be about 67% higher. To alleviate these problems, various research groups have adopted different strategies to improved energy efficiency in electric vehicles to reduce the global warming. The development of higher performance rechargeable battery systems in technology, automotive industries and portable applications will lead to relieve these problems.

The advance in high density battery technology is critical for advancements in a variety of applications ranging from hybrid electric vehicles to consumer electronics. As mention earlier vehicles, domestic purposes, and industries are significant for this technology. One of the principal investigations is the use of different cathode materials to demonstrate the improvements of the energy efficiency of the rechargeable batteries by increasing its capacity. However, not only the performance of these kinds of batteries is critical for its applications in the future, the

production cost, safety and environmental concern is also important. Several materials as cathode for this type of batteries have been provide high voltages and good capacities but full utilization of these materials for numerous recharging cycles and at high discharge currents continue to be a challenge. To meet the futures needs of electrical energy storage is critically to develop novel battery systems that incorporate revolutionary new materials and chemical processes.

1.1 Batteries

A battery is an electrochemical cell that converts stored chemical energy into electrical energy that was invented by Alessandro Volta in 1800. A battery is composed of an anode, cathode, and an electrolyte that allows for ionic conductivity. The anode and cathode are separated by polymeric materials. The schematic and components of an electrochemical cell are shown in Figure 1. There are two types of batteries: primary batteries, which are designed to be used once and discarded when they are exhausted, and secondary batteries, which are designed to be recharged and used multiple times.

Currently, batteries have become a common power source for many household and industrial applications and more strict requirements exist both in energy density and power density of energy storage devices. Also, there is a high demand for high performance batteries. The secondary lithium ion battery is a promising option to meet such demands because of its inherent outstanding characteristics. The lithium ion batteries are discussed below.

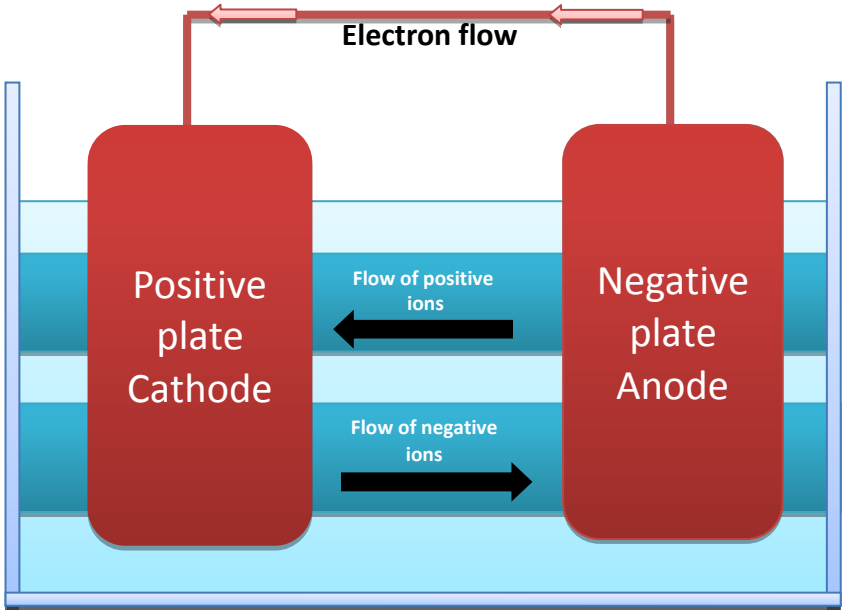

Figure1.1: Schematic of electrochemical cell

1.2 Lithium ion Batteries

The lithium ion battery is a rechargeable battery type in which lithium ions move from the negative electrode to the positive electrode during discharge, and back when charging [2]. The three primary functional components of Li-ion batteries are the anode, cathode and electrolyte. Graphite is the most common anode material. The electrolyte is typically a mixture of organic carbonates. The cathode is significant in determining the capacity of the Li-on battery, as it is the heaviest component; therefore, it has the greatest potential for the improvement of batteries. Lithium is the lightest of all metals, has the greatest electrochemical potential and provides the largest energy density for weight. The chemistry, performance, cost, and safety characteristics are the main advantages of this kind of battery among others. Nowadays, lithium ion batteries are the most common in consumer electronics due to the best energy to weight ratios, no memory effect, and a slow loss of charge when not in use. Recently, the popularity of lithium ion batteries has been increasing for military, electric vehicle, and aerospace applications due to their high energy density. New investigation for this battery is yielding a stream of

improvements to traditional Li-ion batteries technology, focusing on energy density, durability, cost, safety, and active cathode materials. The market for Li-ion batteries is driven by the demand of the portable electronic device market, especially the notebook computer and the cellular telephone. This market has had an explosive growth since 1990 and it is still growing. However, one of the challenges for this technology is to improve the performance of lithium ion batteries to meet increasingly demanding requirements for the latest equipment. To overcome this problem, it is necessary to development a suitable cathode material for the next generations of this battery. The charge and discharge process of the lithium ion batteries is shown in Figure 1.2 and 1.3. As described earlier the cathode materials is a very important part of lithium batteries. Most common cathode materials are described below.

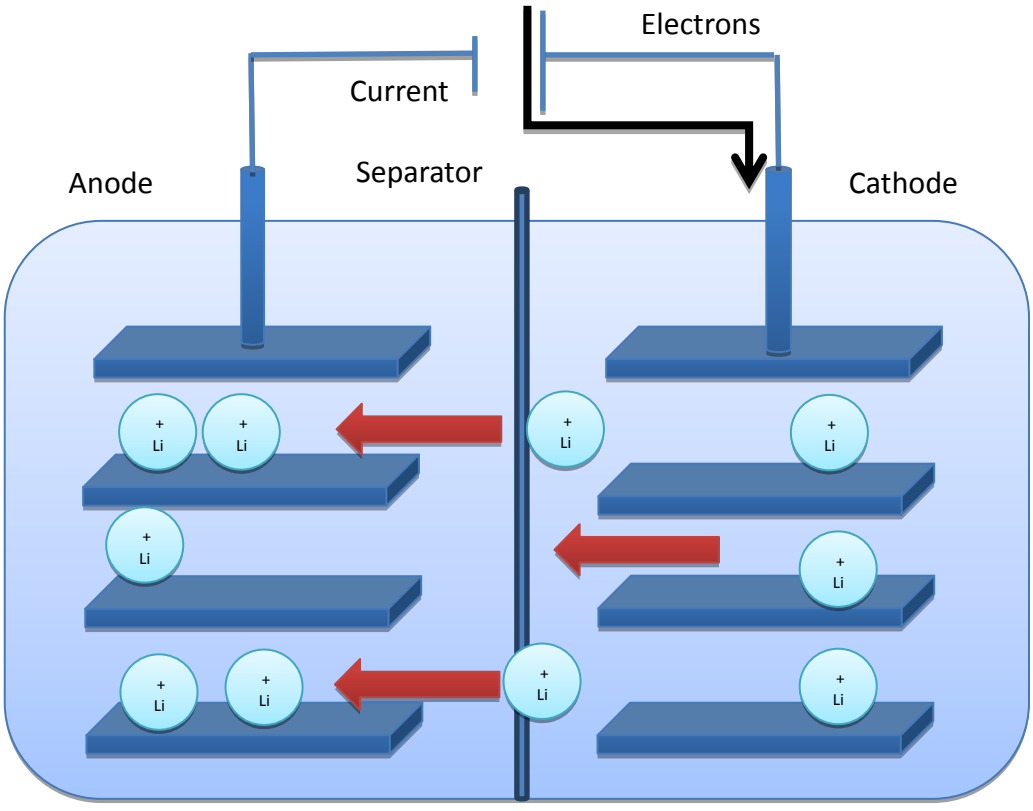

Figure 1.2: Discharge process of Lithium ion battery

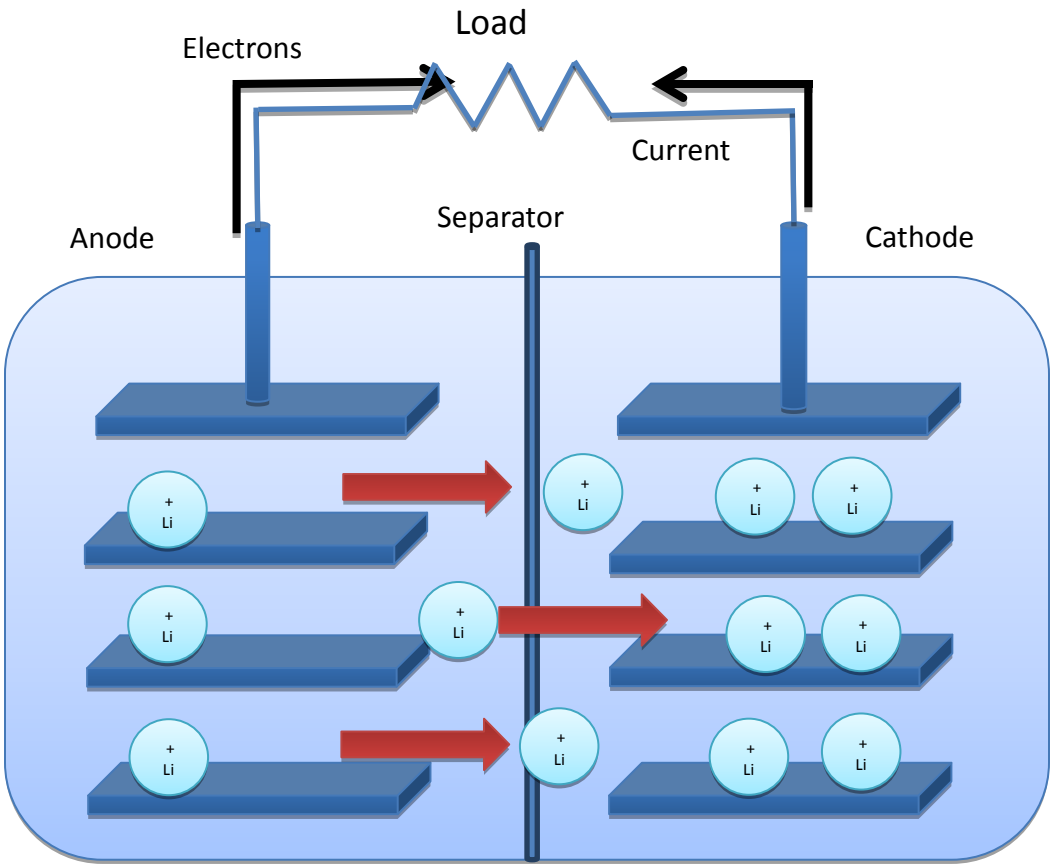

Figure 1.3: Charge process of a Lithium ion battery

1.3 Cathode actives materials for Lithium ion batteries

The successful commercialization of lithium ion batteries for electronics, automobiles, and technology has led to many research groups to invest considerable amount of money in this battery technology that utilizes $LiCoO_2$, $LiNiO_2$, and $LiMnO_2$ cathodes [4]. However, lower cost cathode materials are required for various applications. In addition, these materials limit the applications to small batteries due to the high cost, toxicity, and environmental harmful of the materials. The cathode is particularly critical in determining the capacity of the lithium ion battery, as it is the heaviest component, therefore, it has the greatest potential for the improvement of lithium ion batteries. Cobalt oxide based and materials are dangerous and are

environmentally harmful [5]. Manganese based materials are attractive because of both their low cost and low toxicity. However, they suffer from important capacity fading during cycling, especially at high temperatures and poor low temperature character. These characteristics unfortunately prevent these materials from being used in large scale applications. The improvement of cathode materials is a challenge for meeting current and future energy storage requirements. Currently, several materials are testing to replace current cathodes materials. One of the most promising materials is $LiFePO_4$. The principal properties and benefits of $LiFePO_4$ are described below.

1.4 $LiFePO_4$ for Lithium ion batteries

$LiFePO_4$ has many advantages compared with conventional cathode materials described earlier and it is considered as a promising cathode material because of its theoretical energy density for lithium ion batteries for the next generations of electronic devices [6]. Lithium iron phosphate cell has a discharger potential around 3.4 V vs. lithium [7]. It has received attention as a cathode for Li-ion batteries during the past years, due to the exceptional stability of $LiFePO_4$ at elevated temperatures enables safe, large lithium ion batteries for large scale applications such as electric vehicles or space applications [8]. $LiFePO_4$ can be prepared from different sources, in recent years new synthetic methods are used to reduce the energy consumption, cost, and processing time. In addition, the excellent cycling performance of LiFePO4 in lithium ion batteries at high temperature has been confirmed [9]. However, the main issue of the $LiFePO_4$ is its low conductivity, therefore, many efforts have been devoted to increase and optimize the conductivity of LiFePO4. Currently, there are a lot of different methods to improve the poor conductivity of this material but more investigation is necessary to achieve the ideals results.

Finally, all the materials are inexpensive and with good operability, therefore, it is possible to reach industrial production of $LiFePO_4$ for lithium ion batteries. In Table 1.1 there is a comparison data among various lithium ion batteries.

Table 1.1: Cathode material comparison for Lithium batteries

Battery	**$LiFePO_4$**	**$LiCoO_2$**	**$LiMnO_2$**
Safety	Safest	Not Stable	Acceptable
Environmental	Not Dangerous	Dangerous	Dangerous
Cycle Life	Best	Good	Acceptable
Power Density	Acceptable	Good	Acceptable
Temperature Range	Excellent (-20°C to 70°C)	Decay (-20°C to 55°C)	Decay Fast over 50°C
Cost	Economic	High	Acceptable

1.5 Problems Encountered for $LiFePO_4$

The commercial implementation of $LiFePO_4$ material has been facing problems due to the poor rate capability resulting from its inherent low electronic conductivity (10^{-9} $S{\cdot}cm^{-1}$) and low Li^+ ions diffusion rate [12]. This limitation is its principal drawback and has hindered its wide application in the commercial market. The poor conductivity is because during the lithium insertion and extraction, the resulting phases, $LiFePO_4$ and $FePO_4$ are both poor electronic conductor because they contain Fe cations with only one oxidation state 2^+ and 3^+ respectively [13]. Efforts to optimize the electrical and ionic conductivity of $LiFePO_4$ have focused largely on doping the compound. Chiang and co-worker from MIT increased the conductivity by aliovalent doping. However, doping may have harmful impact if it occurs on the lithium sites.

1.6 History of $LiFePO_4$

John Goodenough discovered $LiFePO_4$ with his research group at the University of Texas at Austin in 1996, as a cathode material for rechargeable lithium batteries [15]. It is a very stable material due to the covalent P-O bonding which stabilize the fully charged cathode versus O_2 release [31]. The theoretical energy density of $LiFePO_4$ is 170 mAh g^{-1} is higher compared with iron based compounds [40]. $LiFePO_4$ which has an ordered olivine type structure has received particular attention during the past years to replace the current cathode material for lithium ion batteries. The main characteristics of $LiFePO_4$ for cathode material are its low cost, non-toxicity, high abundance of iron, its excellent thermal stability, outstanding electrochemical performance, and high specific capacity [47]. The structure of $LiFePO_4$ can be seen in Figure 1.4

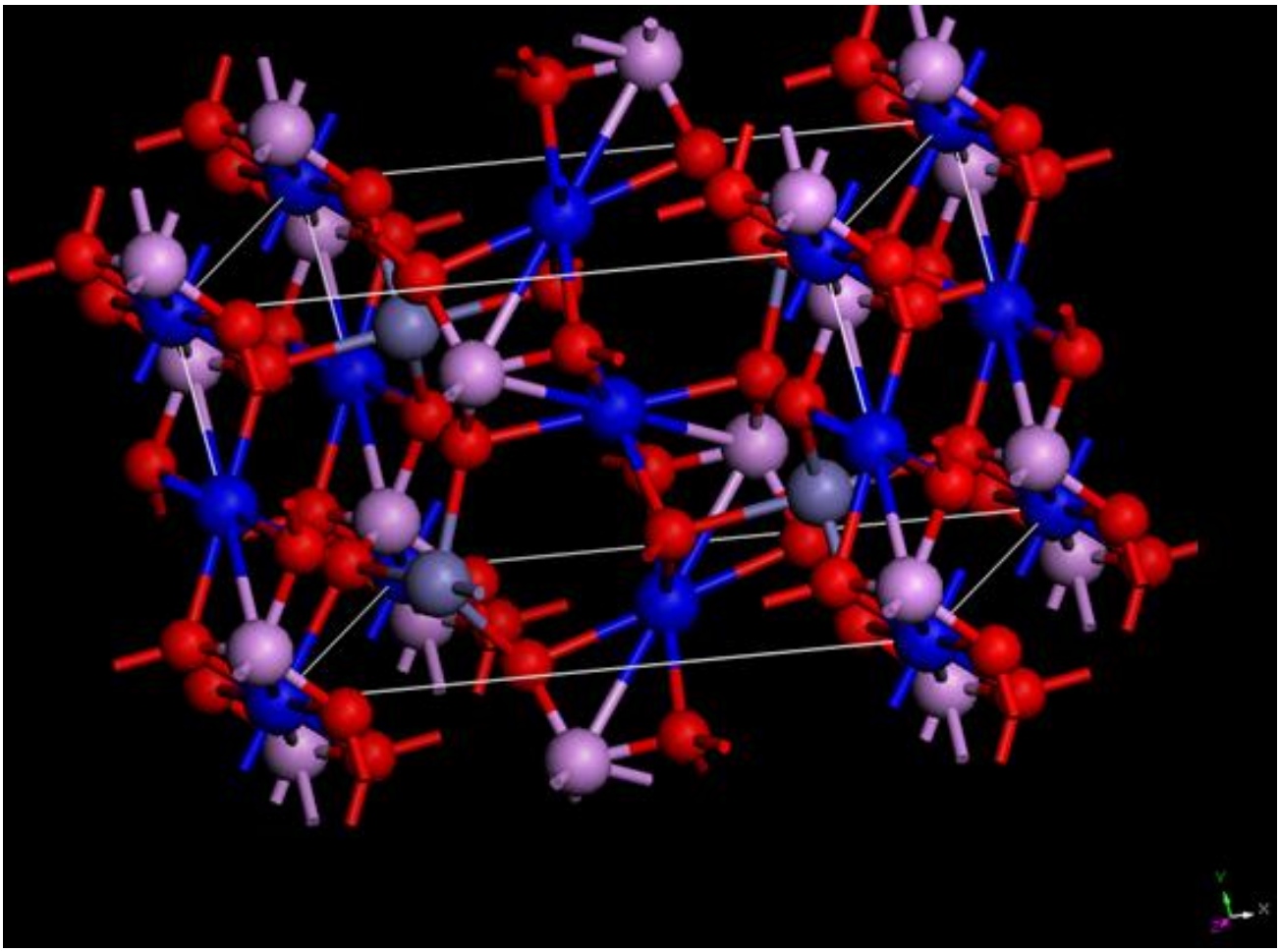

Figure 1.4: The crystal structure of $LiFePO_4$. Purple-Phosphorous, Blue-Li, Grey-Fe, Red-O.

1.7 Objectives

It is clear that $LiFePO_4$ is a viable candidate as cathode active material for Li-ion batteries. The results are wished to be valuable in the further design of the structure of the $LiFePO_4$ cathode materials for lithium batteries of other applications. The following are the specific objectives of the work:

1. Fabricated $LiFePO_4$ thin films using RF magnetron sputtering under varying growth conditions.

2. Study the effect of growth temperature on the structure and electronic properties of $LiFePO_4$.

3. Study the annealing temperature effects on the microstructure and electronic properties of $LiFePO_4$ thin films.

4. Optimized the conditions to high-quality $LiFePO_4$ thin films.

Chapter 2: Experimental

2.1 $LiFePO_4$ Target

$LiFePO_4$ powder was obtained using the solid state route. The obtained powder was mixing with polyvinyl alcohol (PVA) and pressed at 7300 psi for 15 minutes to obtained a pellet. The pellet obained has a 2 inches in diameter and .25 inches of thickness. The formed pellet was sintered during 24 hours at 700°C under normal atmosphere.

2.2 Substrate Cleaning

Silicon wafers and quartz were using in all the experiments. The silicons used were p-type Si (100) wafers. The quartz used were 25mm by 25 mm. To avoid contammination, all the substrates were cleaning before deposition. The silicon wafer were cleaning using the RCA clean procedure to remove all the contamminats. These are the steps for the process:

1. First the silicon wafers were soaked during 5 minutes in methanol, then it was dried by nitrogen.
2. Then, it was soaked in acetone during 5 minutes and rinse with DI water for 5 minutes.
3. Finally it was treated with Buffered Oxide Etch (BOE) to remove any oxide on it.Then it was rinsed in DI water for 5 minutes and dried with nitrogen.

The quartz used were cleaning using a ultasonic bath of methanol and acetone. The quarzt were soaked in methanol during 5 minutes and dried with nigroten. Then they were soaked in acetone for another 10 minutes and dried with acetone.

2.3 Thin Films

The $LiFePO_4$ thin films were grown using a radio-frecuency (RF) sputtering system. Sputter deposition, commonly called sputtering, removes the atoms from the target surface, projecting them into the gas phase from which they condense on another surface. Usually Ar flows into the chamber, the chamber is evacuated to high vacuum usually 10^{-6} Torr. The Ar gas will be ionized to create Ar^+ plasma. Ar^+ ions accelerate towards cathode, under the influence of cathode voltage, and bombard the target ejecting a target atom. These target atoms will be deposited on to the substrate placed above the target to form the film. The sputtering process is shown in Figure 2.1.

The deposition system used for all the depositions was Kurt J Lesker sputter machine (Figure 2.1). During R.F. magnetron sputtering, the distance between the target and the substrate was 8 cm. As described earlier the substrates used were silicon wafers and quartz. The sputtering gas was high purity Ar with 99.999% purity, the gas total flow was set at 50 sccm. An R.F magnetron sputtering power of 40 Watts was applied to the target. Before deposition of the films, the target was pres-puttered for 10 minutes in order to remove any contaminant atoms from the chamber and target. During deposition, the substrates were grown at various temperatures, from RT to 500 °C. To increase the temperature of the substrates halogen lamps were used, and they were controlled by Athena X25 system until they reached the desired temperature. The prepared $LiFePO_4$ thin films were annealed at 400°C, 500°C, 600°C, 700°C, and 800°C for 1 and 2 hours using a furnace. The deposition and annealing conditions are described in Table 2.1 and 2.2 respectively.

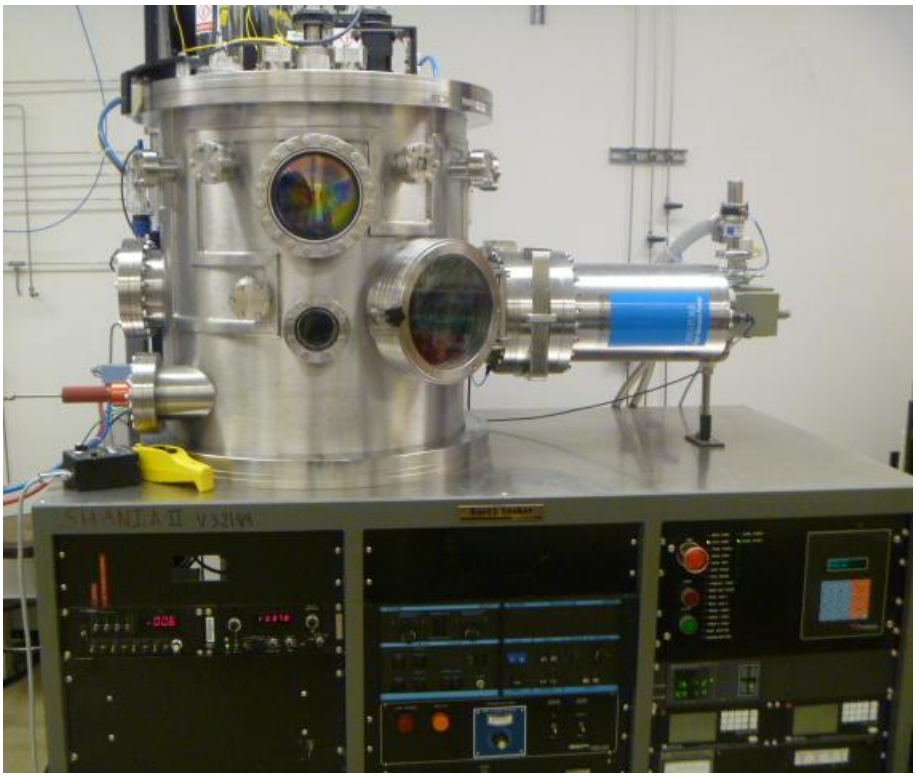

Figure 2.1: Kurt J Lesker sputter system.

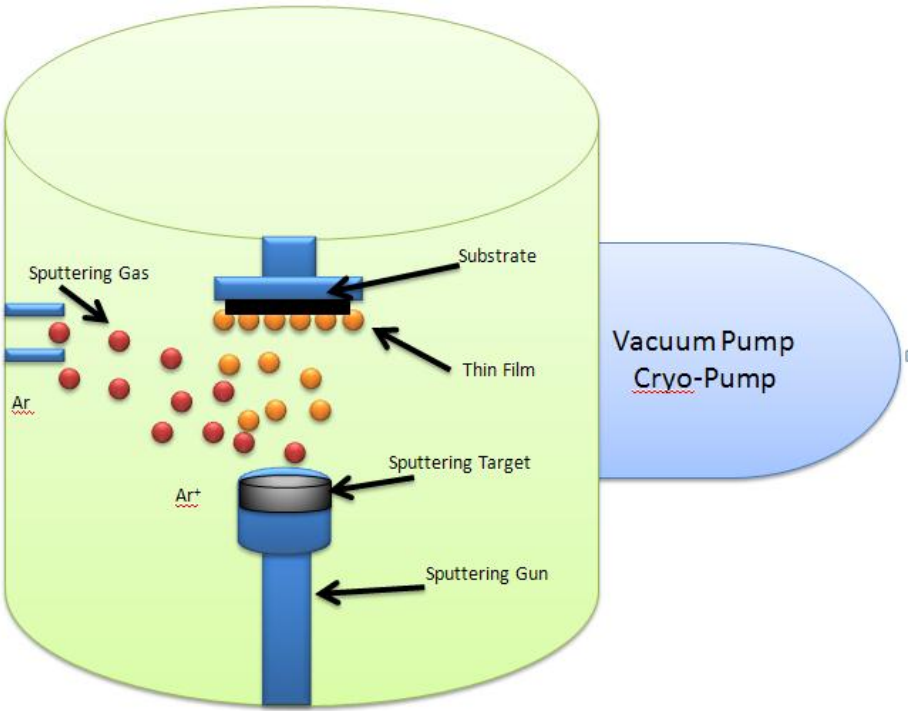

Figure 2.2: Sputtering Process

Table 2.1: Deposition Conditions

Sample	Sample Name	Total Pressure (Torr)	Argon Flow (sccm)	Temperature (^{0}C)	Power (Watts)	Deposition Time (hr)	Distance Target to Substrate (cm)
1	LiFEPO4-SQ1	2.1X10E-3	50	RT	40	1	8
2	LiFEPO4-SQ2	2.2X10E-3	50	100	40	1	8
3	LiFEPO4-SQ3	2.4X10E-3	50	200	40	1	8
4	LiFEPO4-SQ4	2.1X10E-3	50	300	40	1	8
5	LiFEPO4-SQ5	2.3X10E-3	50	400	40	1	8
6	LiFEPO4-SQ6	2.1X10E-3	50	500	40	1	8

Table 2.2: Annealing Conditions

Sample	Sample Name	Temperature (^{0}C)	Deposition Time (hr)
1	LiFEPO4-SQ1	400	1
2	LiFEPO4-SQ1	500	1
3	LiFEPO4-SQ1	600	1
4	LiFEPO4-SQ1	700	1
5	LiFEPO4-SQ1	800	1
6	LiFEPO4-SQ2	400	1
7	LiFEPO4-SQ2	400	2
8	LiFEPO4-SQ2	500	2
9	LiFEPO4-SQ2	600	2
10	LiFEPO4-SQ2	700	2
11	LiFEPO4-SQ2	800	2

2.4 Surface Morphology

The surface morphology of $LiFePO_4$ thin films was obtained using a HRSEM. The information about the microstructure of the thin films was found using the surface morphology. In addition, the information about the thin film and substrate interaction was obtained using the

interface analysis. The HRSEM used in this work was a Hitachi S-4800 electron microscope (Figure 2.3).

Figure 2.3: Hitachi S-4800 electron microscope

The SEM electron beam is produced via an electron gun or filament. A voltage is applied to the filament which acts like a cathode, causing it to heat up. When the filament gets hot enough, electrons are emitted thermionically. A strong electric force is present between the electrons emanating from the filament and the anode plate. This force causes the electrons to be accelerated towards the anode plate. In fact, some of the thermionic electrons are accelerated in such a manner as to stream right by the anode plate and down the column of the microscope to the sample. This electron beam is scanned back and forth over the surface of the specimen using electromagnetic lenses and the electrons that are reflected from the specimen are used to resolve an image on the computer monitor. SEM must be carried out under a high vacuum such as 10^{-}

^{6} Torr or better. In Figure 2.2 one can see the schematic sketch of an (SEM) showing its major components.

Analysis software is used to determine the grain size and thickness of the thin film. To acquire the image of the surface the sample is placed on a flat stage with its film surface facing the beam. For the interface image or cross section, the sample is placed in a way that both the film and the substrate are facing the beam.

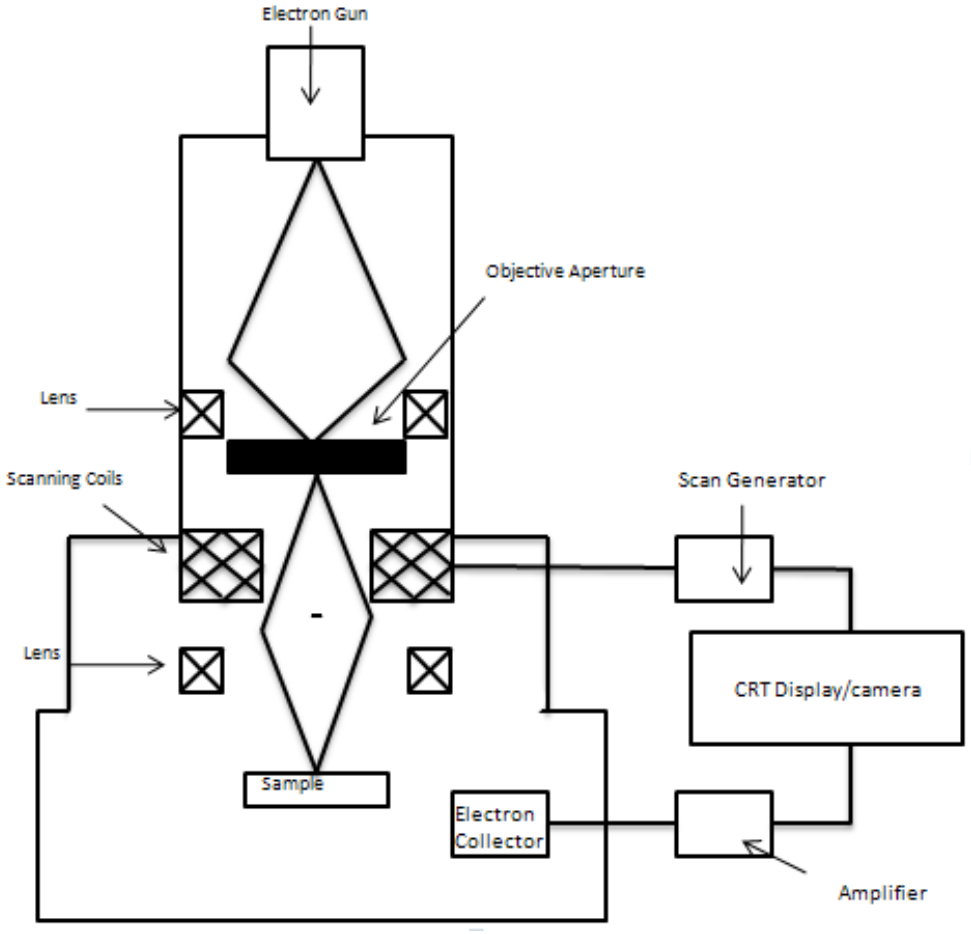

Figure 2.4: Schematic of Scanning Electron Microscopy (SEM)

2.5 Structural Characterization

The XRD pattern of the sample was obtained using a Bruker D8 advance x-ray diffractometer (Figure 2.5) employing Cu Kα radiation (1.54 Å). The crystal structure, crystallite size, and the phases of the thin films were determined from XRD patterns. X-ray powder diffraction (XRD) is a rapid analytical technique primarily used for phase identification of a crystalline material and can provide information on unit cell dimensions such as lattice parameter, d-spacing, film orientation. The XRD operates based in the Bragg's Law [57].

$$\lambda = 2dSin\theta \ldots\ldots\ldots\ldots\ldots\ldots\ldots\ldots (1)$$

where λ is the wavelength, d is the inter planar distance, and Θ is the angle.

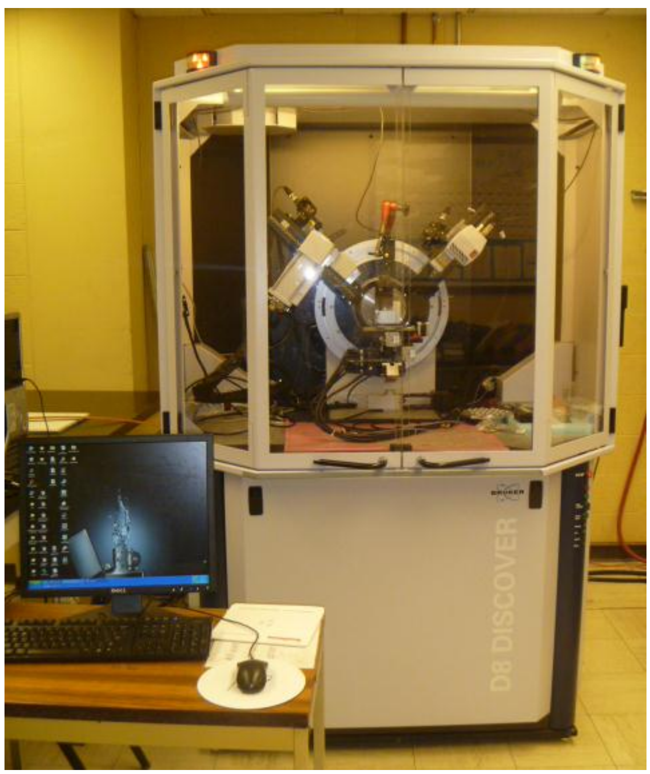

Figure 2.5: Bruker D8 advance x-ray diffractometer

2.6 Optical Characterization

The samples obtained have been characterized using a Cary 5000 UV-VIS-NIR optical spectrophotometer. The transmittance of a sample is the ratio of the intensity of the light that has passed through the sample to the intensity of the light when it entered the sample. The transmittance data obtained for the samples is used for calculating the band gap. First, the absorption coefficient has to be determined. The absorption coefficient determines how far into a material, light of a particular wavelength can penetrate before it is absorbed. It is determined using the thickness of the film (t) and transmittance data (T) from the formula [50].

$$\alpha = \frac{-\mathrm{Ln}(T)}{t} \ldots\ldots\ldots\ldots\ldots\ldots\ldots\ldots\ldots\ldots\ldots\ldots\ldots\ldots\ldots\ldots\ldots\ldots\ldots\ldots\ldots\ldots (2)$$

The energy of the photons (hv) is calculated at every wavelength of light using the following equation

$$hv = \frac{1240}{\lambda} \ldots\ldots\ldots\ldots\ldots\ldots\ldots\ldots\ldots\ldots\ldots\ldots\ldots\ldots\ldots\ldots\ldots\ldots\ldots\ldots\ldots\ldots\ldots (3)$$

Finally, the optical band gap energy was estimated from transmittance spectra by assuming that the absorption coefficient α is given by the following equation [51]

$$\alpha hv = B\left(hv - E_g\right)^2 \ldots\ldots\ldots\ldots\ldots\ldots\ldots\ldots\ldots\ldots\ldots\ldots\ldots\ldots\ldots\ldots\ldots\ldots\ldots\ldots\ldots\ldots (4)$$

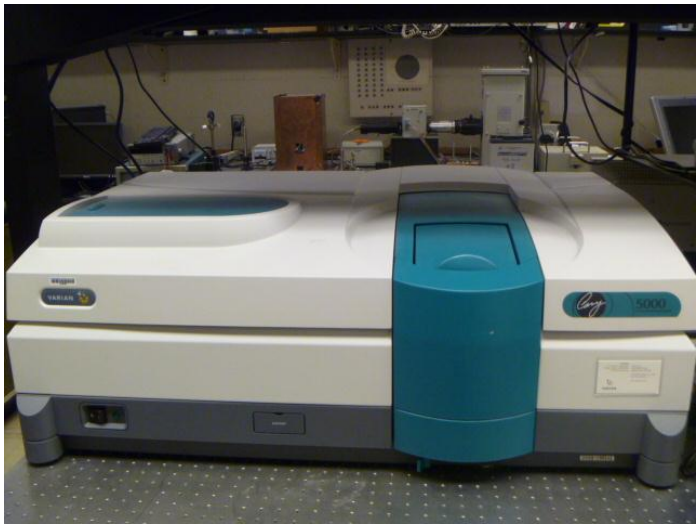

Figure 2.6: Cary 5000 UV-VIS-NIR optical spectrophotometer

Chapter 3: Literature Review

Padhi et al. [15] have demonstrated in 1996 that $LiFePO_4$ could be used as an active cathode material in lithium ion rechargeable batteries. The advantages of this $LiFePO_4$ compared to other ion based compounds for high density batteries such as, cost, toxicity, theoretical capacity and electrochemical performance were discussed. The pioneering work of this research group at University of Texas at Austin attracted the attention of electromechanical and energy research community worldwide and generated a strong interest in this material

Takahashi et al. [5] disscused the effect of operating temperature of $LiFePO_4$ used as cathode material. It was showed that the cell capacity increases as the cell operating temperature is raised because the lithium ion diffusion in the $LiFePO_4$ particles is enhanced. They found that electrochemical lithiation and delithiation occurs as a two-phase reaction and the structure of the delithiated product is similar to heterosite, the same as that of chemically delithiated product. Good reversibility is expected from the small structural change between $LiFePO_4$ and $FePO_4$, which coexist during lithium insertion and extraction.

Prosini et al. [6] suggested that the capacity of $LiFePO_4$ can be greatly improved by the addition of fine particles of carbon black during its synthesis. Improvements in the rate capability have also been achieved by synthesizing small particles and by the addition of silver or copper. It was reported that a specific capacity of 120 mAh g^{-1} can be obtained at a high rate.

Ravet et al. [11] improved significantly the electrochemical performance of $LiFePO_4$ by applying carbon coating. Yamada et al. [14] reported that increase in the specific surface area resulting from very fine and uniform particles gives good electrochemical cycle performance. He also obtained capacities as high as 165 mAh/g.

Xia et al. [17] discussed the effect of surface area. It was found that the rate capability of LiFePO4 is mainly controlled by its specific surface area and it is an effective way to improve the rate capability of the sample by increasing its specific surface area. $LiFePO_4$ prepared with a high specific surface area of 24.1m^2 g^{-1} has an excellent rate capability and can deliver 115 mAh g^{-1} and 145 mAh g^{-1} of reversible capacity even at the 1C and 5C rates respectively. The results showed that by increasing the specific surface are, the electrochemical performance can be improved.

Kim et al. [19] prepared $LiFePO_4$ powder at 700 ◦C. It showed a higher capacity compared with powders prepared at 600 and 800 ◦C. This is because it has a well-developed crystalline structure and optimum particle size. At high operating temperatures, the capacity of a $LiFePO_4$ cell is increased, however, there is a low conductivity of the powder. This problem can be solved by increasing the conductivity of the powders by using a more suitable conductive additive.

Sang et al. [23] prepared $LiFePO_4$ by mechanical alloying (MA). It showed a maximum discharge capacity of 135mAh g−1 at the C/20 rate (8.5mAg−1) when fired at a relatively low temperature of 600 ◦C. The composite also displays a better rate capability, a higher charge and discharge capacity and a more stable cycle-life than when produced by the conventional solid-state method. The improved electrode performance of MA samples originates mainly from very fine particles of sub-micron size and with a rough surface morphology. These powder characteristics increase the surface area of $LiFePO_4$ particles and maximize the contact area with the conductor additive, which results in enhanced electronic conductivity. It is concluded that fine particle size and uniformly dispersed carbon black between the particles achieved with the MA process increases the electronic conductivity.

Ceder et al. [34] based on phase diagram reported that a fast Li^+ ion conductivity phase prepared by a controlled off stoichiometry method on the surfaces of $LiFePO_4$ particles less than 500nm to display rate capability equivalent to full battery discharge.

Li et al. [35] used the pressure pulsed chemical vapor infiltration (PCVI) technique, to deposited pyrolytic carbon films on the surface of $LiFePO_4$ particles for cathode material of lithium-ion batteries. All the PCVIed samples exhibited excellent rate performance. The specific capacities of the samples were maintained at 117, 124 and 132 mAh g−1, respectively, which were 120.8, 264.7 and 29.47% larger than those of corresponding original $LiFePO_4$, respectively, at a 5C rate at 55 ◦C. The electrochemical performance of $LiFePO_4$ electrodes is improved significantly for the PCVIed samples.

Rousse et al. [36] reported neutron diffraction results from polycrystalline samples, confirming the collinear structure below T_N=52 K. Santoro et al. [12] studied the magnetic properties of $LiFePO_4$ and showed that its space group is Pnma. The magnetic results showed a paramagnetic-antiferromagnetic phase transition. Denis et al. [32] also discussed the magnetic properties of this compound. His results showed that the ground state of $LiFePO_4$ is a collinear antiferromagnet and very robust against crystal imperfections.

Xian-Juan et al. [45] prepared thin films by radio frequency magnetron sputtering. It was found that when the temperature increased, the thin film structure change form amorphous to crystalline. However, at high temperatures an impurity phase can be developed. Chiu et al. [46] showed that thin films of carbon mixed with $LiFePO_4$ prepared with inductively coupled plasma (ICV) exhibited higher specific capacity that can be related to the film structure and surface morphologies.

Sauvage et al. [48] prepared free carbon $LiFePO_4$ thin films using the Pulsed Laser Deposition (PLD) technique. It clearly showed that once again the main limitation of this compound is its low conductivity with the main limitation being the ionic conductivity. The results demonstrated that thin film approach is very valuable to understand electrode material limitations. Tang et al. [49] also discussed $LiFePO_4$ thin films prepared using (PLD) technique. He showed that the influence of deposition parameters, e.g. substrate temperature, argon pressure, and annealing modify the crystalline, surface morphology, and the electrochemical properties of the compound.

Numerous studies have been devoted to understand and establish the relation between the deintercalation and intercalation process in $LiFePO_4$. Islam et al. [54] have shown that the lithium ions can move easily in the tunnels parallel to the b direction. However, Maier et al [52] showed that the electronic conductivity, ionic conductivity, and chemical diffusion of lithium ions are essentially two dimensional b-c plane in the $LiFePO_4$ single crystal.

Chapter 4: Results and Discussion

The purpose of the research work is to perform fabrication, microstructure analysis, and electronic property measurement of $LiFePO_4$ thin films for application in high-energy density microbatteries. This chapter discusses the results obtained in the following sequence. X-ray diffraction (XRD) measurements are first discussed to establish the effect of substrate temperature on the crystal structure and phase formation. Subsequently, the scanning electron microscopy (SEM) data are presented to discuss the grain structure and surface morphology evolution. Energy dispersive x-ray spectrometry (EDS) data are presented following the SEM analyses to establish the chemical composition or phase of $LiFePO_4$ films. After that, the optical properties are discussed to show the electronic structure of $LiFePO_4$ films as a function of growth temperature. The electrical properties are presented and explained following optical properties. An emphasis is made to establish a correlation between growth conditions and electronic properties of $LiFePO_4$ thin films. This is very important since most of the applications of $LiFePO_4$ depend on its microstructure and electronic properties. Also, the ability to tailor the microstructure and properties so as to optimize electrochemical performance requires a detailed fundamental understanding of $LiFePO_4$ thin films.

4.1 Crystal Structure

The XRD patterns of $LiFePO_4$ thin films are shown in Figures 4.1 and 4.2. The XRD patterns of bulk $LiFePO_4$ are shown in Figure 4.1. $LiFePO_4$ was found to form in the Pnma space group with olivine-type structure without any impurity phase. The calculated values of the lattice constant is a=10.4093Å, b=6.0500Å and c=4.7315 Å [6], which are slightly higher than that of the reported values. Figure 4.2 shows the XRD spectra of the $LiFePO_4$ thin films post-fabrication

annealed at different temperatures. $LiFePO_4$ thin films grown or annealed at temperatures T ≤ 500 °C did not show any features and are completely amorphous. Onset of crystallization is noticed in the $LiFePO_4$ thin films when annealing was performed at 600 °C. It can be seen that the XRD spectra show crystalline features for $LiFePO_4$ thin films annealed at 600 ^oC. The peak at 2Θ=21.5° corresponds to the diffraction from (111) planes. The intensity of this peak increases with further increase in the annealing temperature. It is evident (Fig. 4.2) that for the films post annealed at 600–800 °C, the (111) peak shows the highest intensity.

The results indicate that annealing at 600 ^oC promotes the crystallinity and development of (111) orientated structure of $LiFePO_4$ thin films. The (101) plane is parallel to the a and b axis in the $LiFePO_4$ olivine structure, which is more stretchable as observed during the Li^+ intercalation and de-intercalation process [45]. As a consequence, grains with (101) plane parallel to the substrate are slightly more favorable.

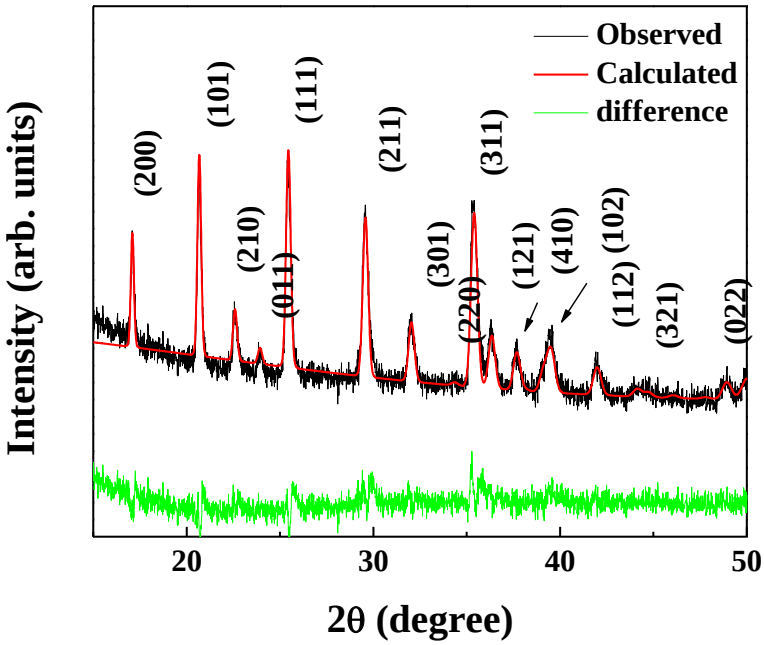

Figure 4.1: XRD pattern of $LiFePO_4$ bulk

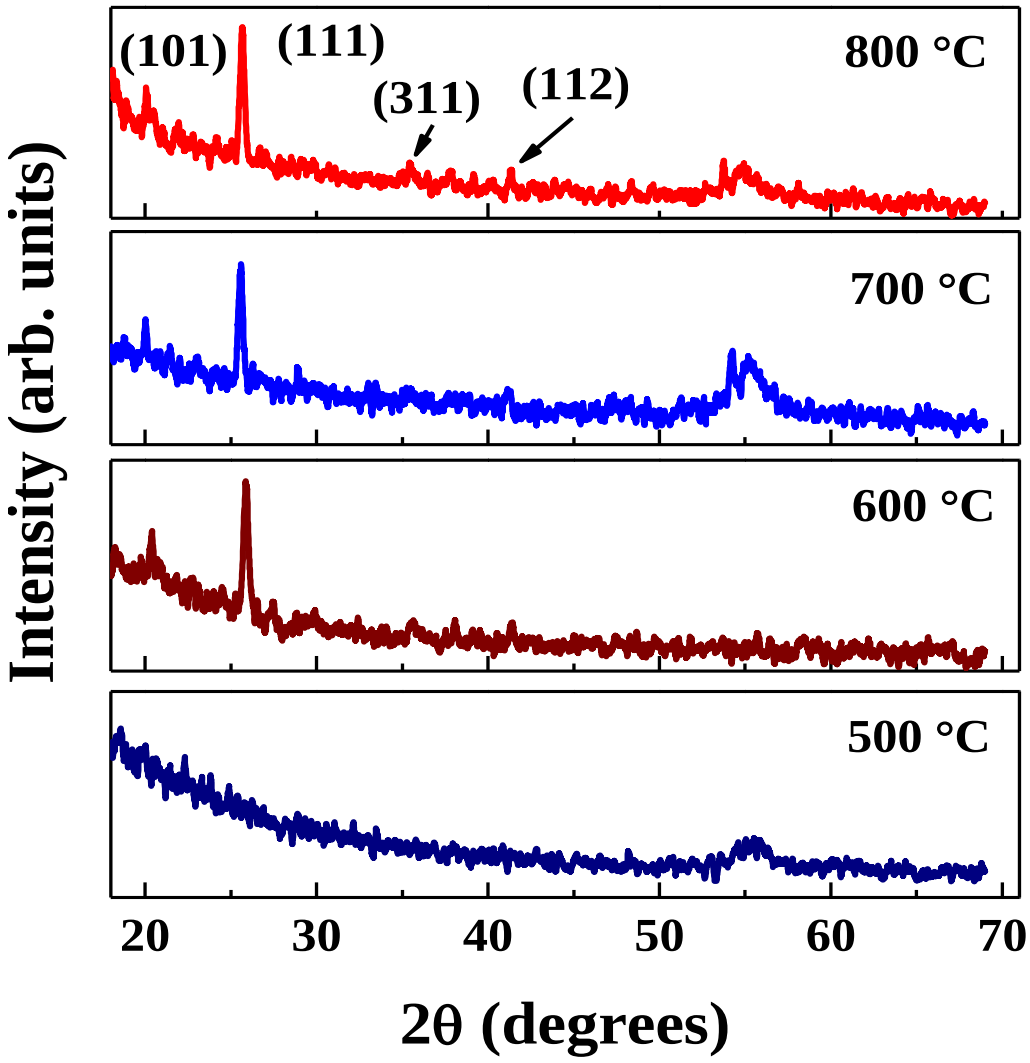

Figure 4.2: XRD pattern of $LiFePO_4$ thin films

4.2 Surface Morphology

The scanning electron microscopy (SEM) images of $LiFePO_4$ thin films as a function of substrate temperature T_s are shown in Figures 4.3 and 4.4. The effect of temperature on the surface morphology of the thin films is significant. The images show no features for $LiFePO_4$ films grown at $T_s \leq 500$ °C even at very high magnifications. The thin films were grown from RT to 500°C. The images are in agreement with the XRD results indicating the complete amorphous nature of the samples. However, as seen in SEM images, some micro-cracks develop on the film

surfaces. It can be attributed to severe ion bombardment induced plasma damage. It has been reported that the finer grain size shortened transport length of lithium ions and therefore improved electrochemical performance of $LiFePO_4$ [39]. Preliminary studies on the sputtered thin films show that the substrate temperature has a strong effect on the morphology and the electrochemical characteristics of LiFePO4 thin films. The texture of LiFePO4 thin films has a significant effect on the electrochemical properties [47].

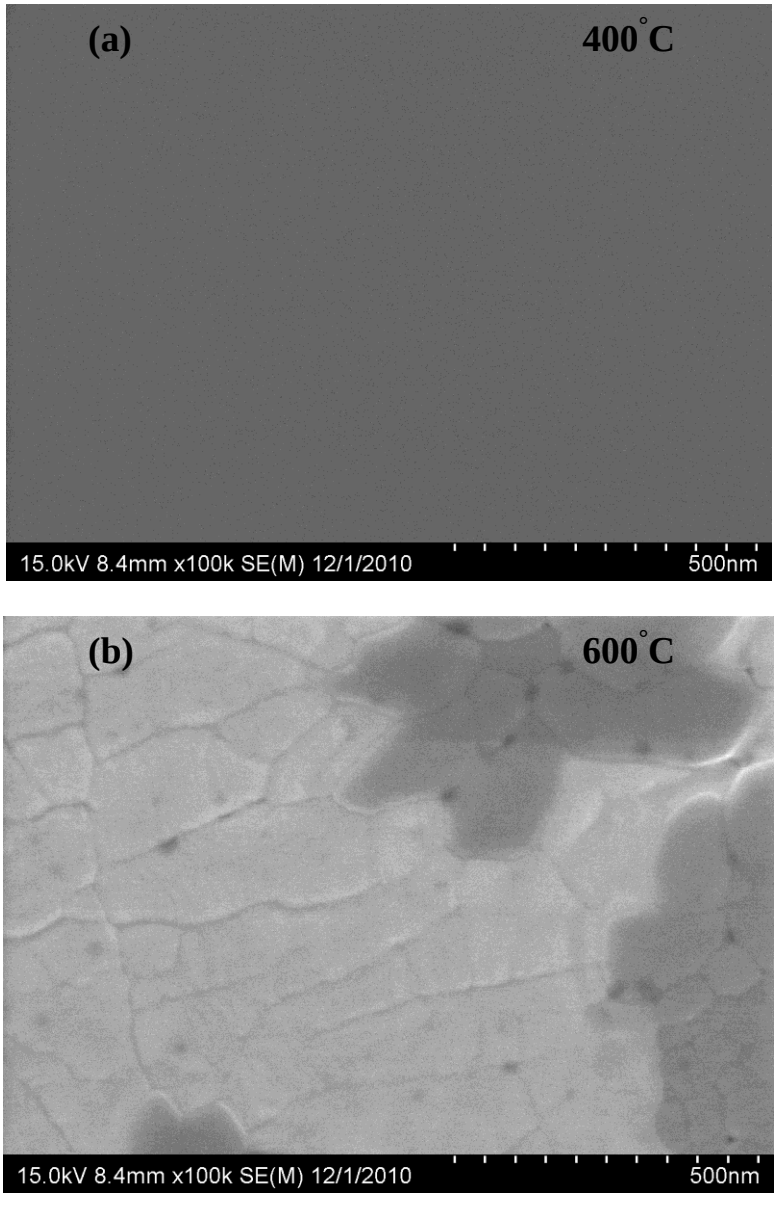

Figure 4.3: SEM images of $LiFePO_4$ thin films

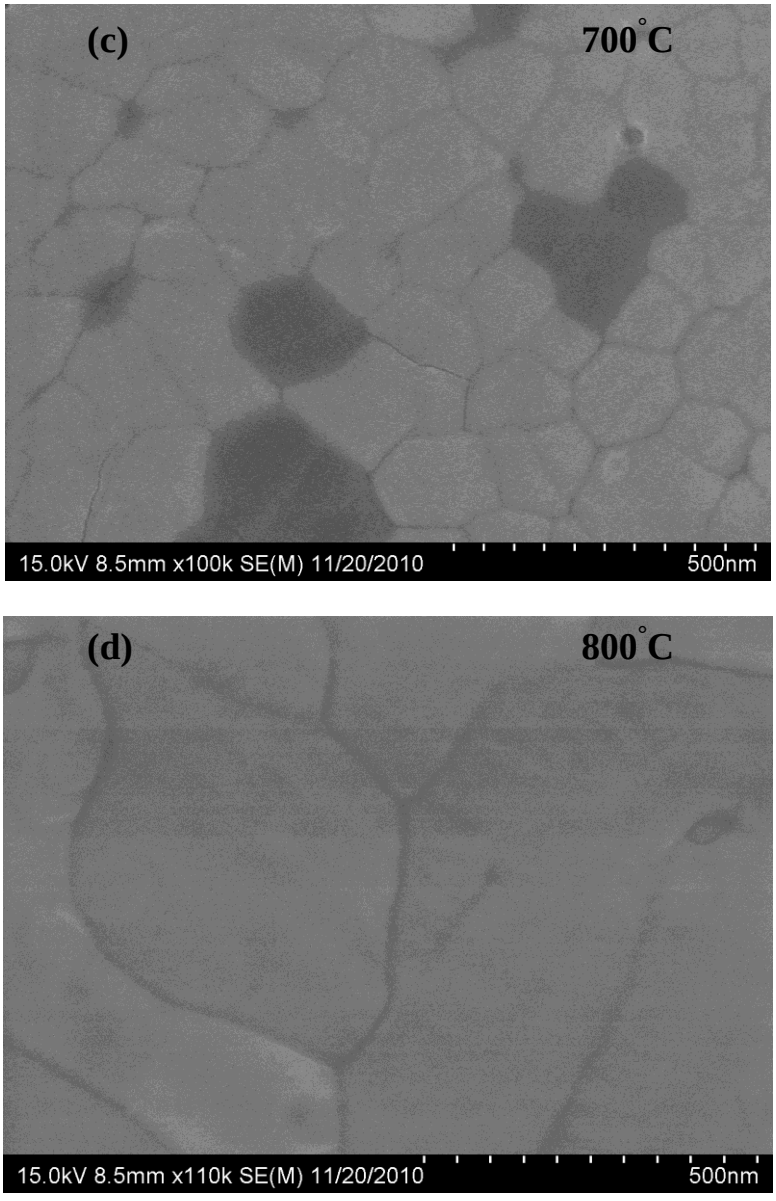

Figure 4.4: SEM image of $LiFePO_4$

The results from XRD and SEM suggest that a further increase in temperature beyond 600 °C results in changes in the crystal structure and morphology. $LiFePO_4$ films continue to show preferred growth along with an increase in average particle size with increasing temperature. These results suggest that an optimum substrate temperature is essential to obtain well crystallized $LiFePO_4$ thin film.

4.3 Chemical Composition

The energy-dispersive X-ray (EDS) spectra of representative $LiFePO_4$ films as a function of annealing temperature are shown in Figure 4.5. The spectra indicate the characteristic x-ray peaks corresponding to O, P, and Fe atoms present in the sample. The absence of Li is because the materials cannot be detected by the EDS. No other elements were detected, which is a sign of high purity $LiFePO_4$ and without any elemental impurities incorporated from chemical processing or post-annealed.

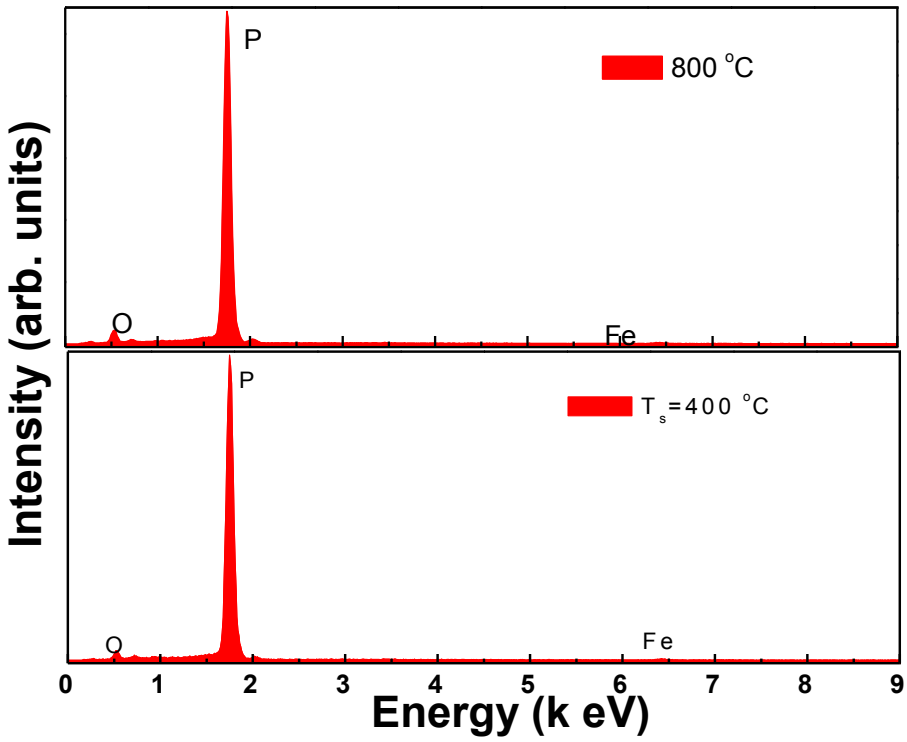

Figure 4.5: $LiFePO_4$ films EDS spectra at various temperatures

4.4 Optical Properties

The optical transmittance spectra of $LiFePO_4$ films are shown in Figure 4.6 to 4.8. The spectral transmittance characteristics of $LiFePO_4$ films as a function of substrate temperature (T_s)

exhibit interesting features. The spectral transmittance in general increases with increasing T_s. In the visible to near infrared regions of the spectrum, the transmittance of these films is found to be generally high. The on-set of a sharp decrease in the spectral transmittance towards ultraviolet regions of the spectrum is due to fundamental absorption of the incident energy across the band gap of the material. It can be seen that this absorption edge is shifting towards shorter wavelength side with increasing T_s. This feature is an indicative of the electronic structure changes in the $LiFePO_4$ films with increasing T_s.

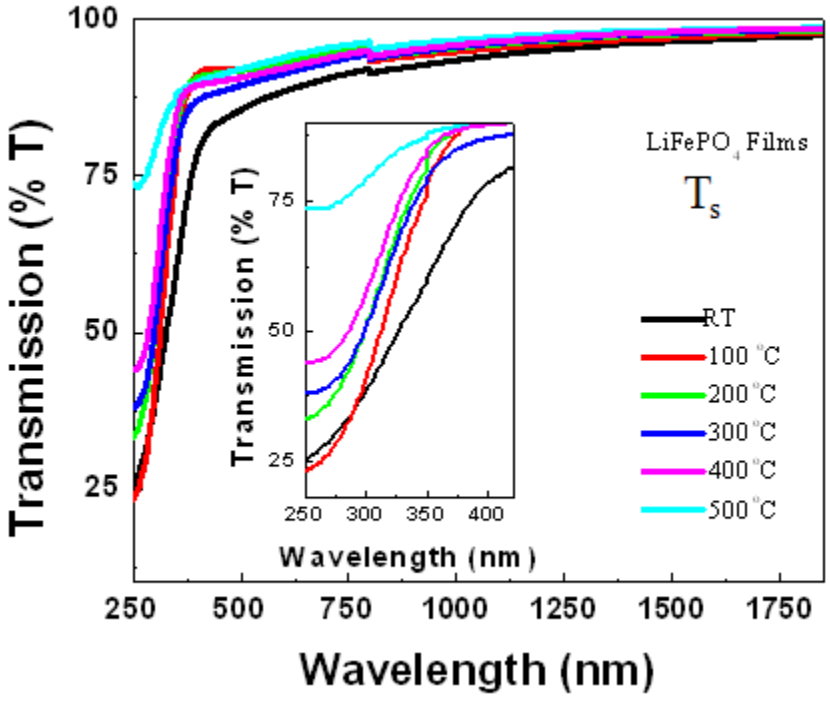

Figure 4.6: Optical transmittance spectra of $LiFePO_4$ films.
Inset the visible spectrum.

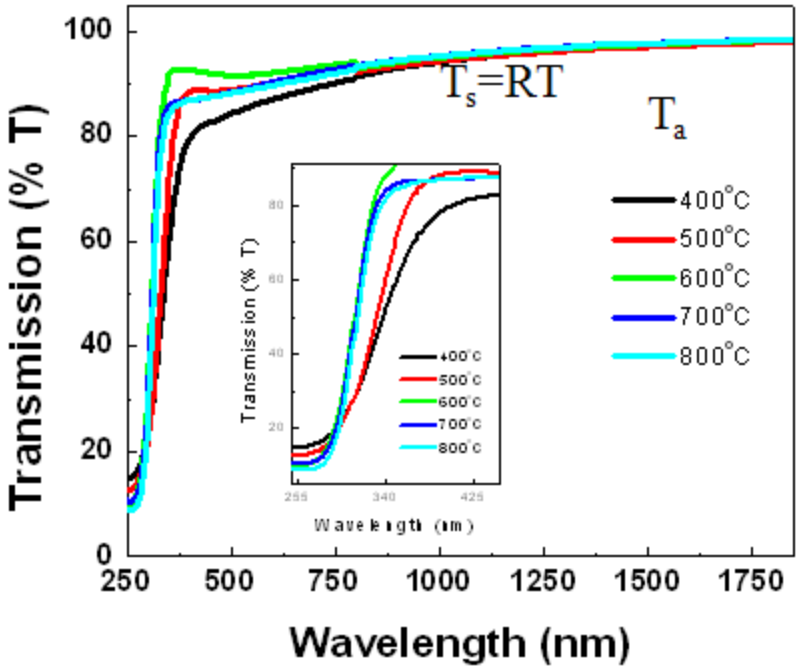

Figure 4.7: Optical transmittance spectra of $LiFePO_4$ films. Annealing 1 hour. Inset the visible spectrum.

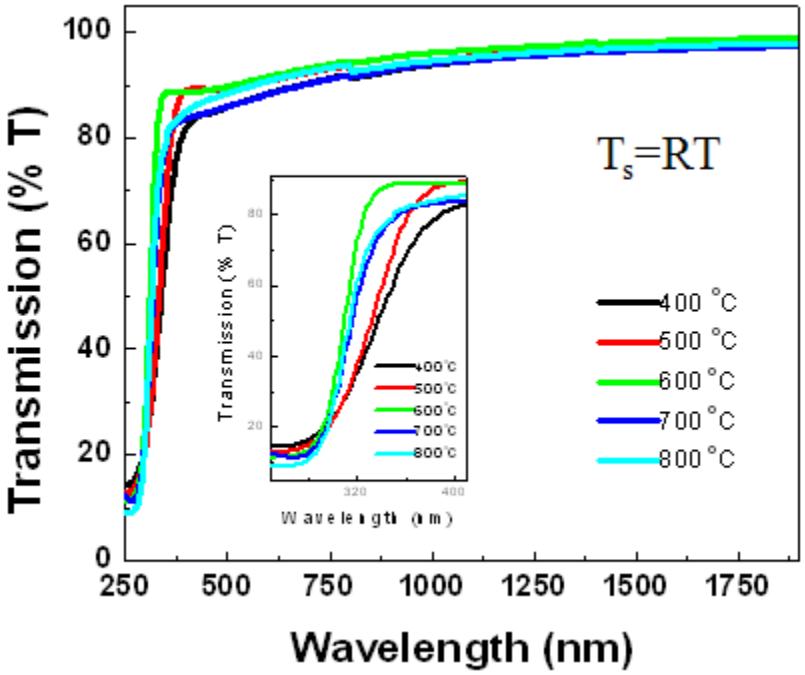

4.8: Optical transmittance spectra of $LiFePO_4$ films. Annealing 2 hours Inset the visible spectrum.

The optical band gap energy was estimated from transmittance spectra. It is known that the optical absorption below E_g follows an exponential behavior. The absorption, therefore, is exponentially dependent on the energy (hv) of incident photon in that region. For $LiFePO_4$, in the E_g region or above the fundamental absorption edge, the absorption follows a power law of the form [50, 51]:

$$\alpha hv = A\left(hv - E_g\right)^2 \quad \text{……………………………………………………} (5)$$

where A, hv, and Eg are a constant of proportionality, photon energy and optical band gap energy, respectively. The optical band gap values were calculated for the films with different thickness. The optical absorption coefficient (α) was determined using the relation [48];

$$\alpha = 2.303 \frac{\log_{10}[(1-R)^2/\ T]}{d} \quad \text{…………………………………………} (6)$$

where R is the reflectance, T is the transmittance and d is the thickness of the film. The optical energy gap of a given film is found by plotting $(\alpha hv)^{1/2}$ versus *E* and extrapolating linear portion of the curve to α=0.

The absorption data and the plots obtained for $LiFePO_4$ films are shown in Figures 4.9, 4.10, and 4.11. The E_g values were determined by extrapolating the linear region of the plot to hv = 0. From RT- 500 °C E_g increases from 2.5 to 3.25 eV with increasing T_s. The same results occur with the annealing samples. The T_s and E_g relation is shown in Figure 4.11. The highest values were obtained with the annealing samples. The maximum value 3.75eV was obtained when T_s was annealing at 600°C for 2 hours.

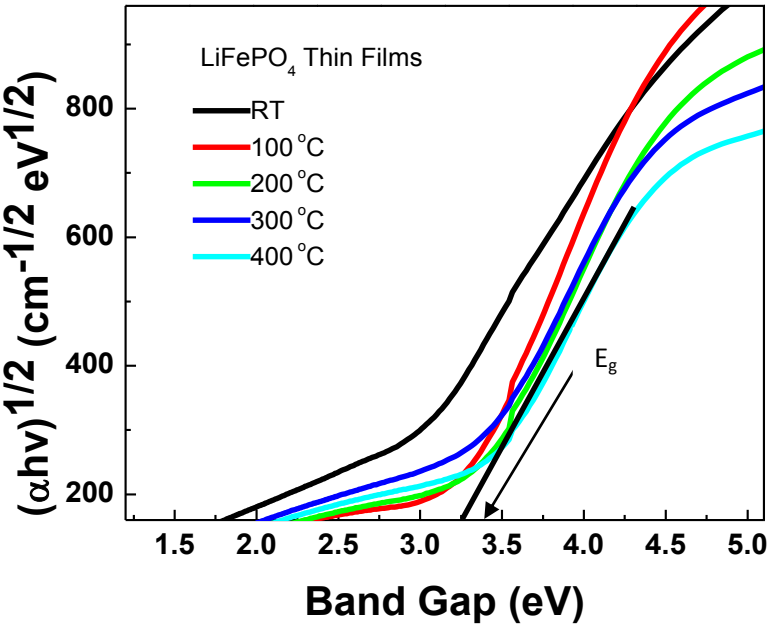

Figure 4.9: $(\alpha h\nu)^{1/2}$ vs. hv plots for $LiFePO_4$ films. Linear fits of the absorption data indicate the indirect band gap of $LiFePO_4$ films. The E_g values determined by extrapolating the linear region of the plot to hv = 0

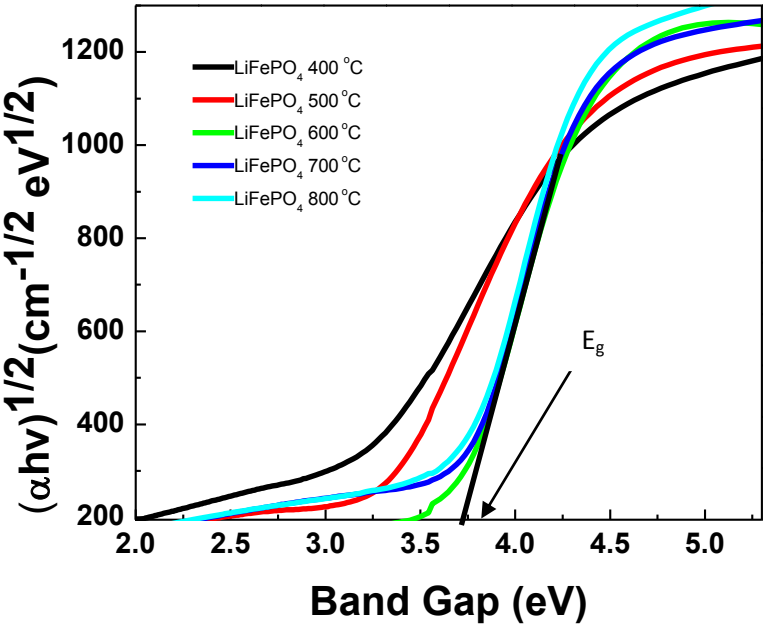

Figure 4.10: $(\alpha h\nu)^{1/2}$ vs. hv plots for $LiFePO_4$ films. Annealing 1 hour

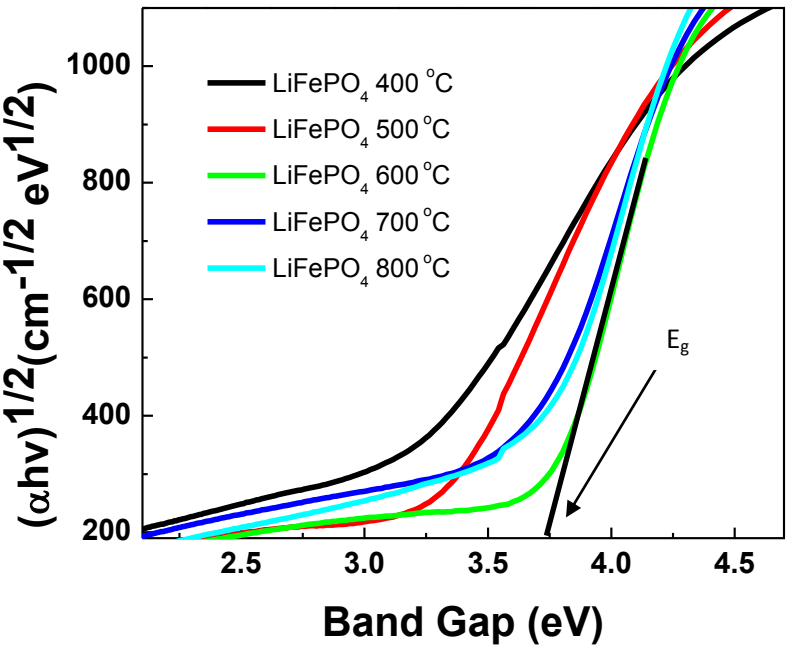

Figure 4.11: $(\alpha hv)^{1/2}$ vs. hv plots for $LiFePO_4$ films. Annealing 2 hours

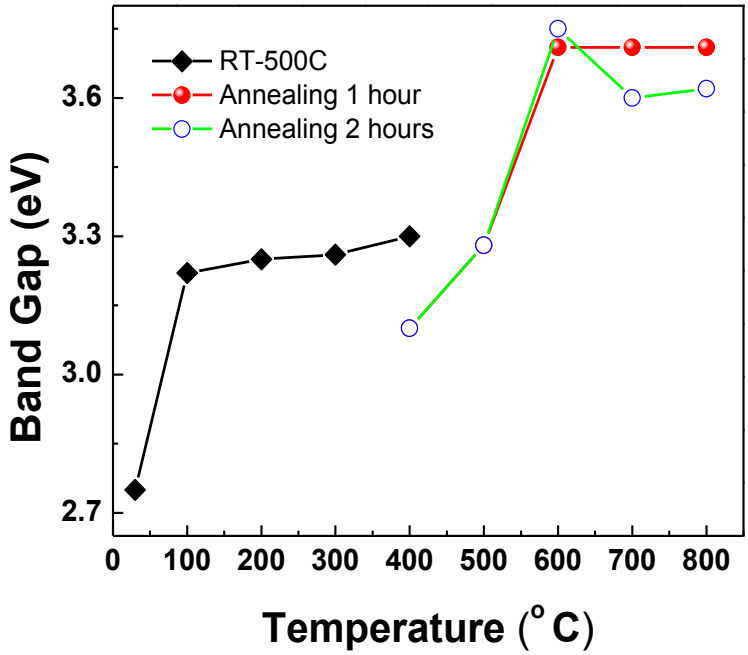

Figure 4.12: T_s-E_g and T_a-E_g relationship in $LiFePO_4$ films.

The results indicate that the microstructure has significant effect on the optical properties of LiFePO4 films. The films annealed from 600-800 °C show higher band gap energy. The film annealed at 600 °C for 2 hours has the highest band gap.

4.5 Electrical Properties

The room temperature electrical conductivity variation of $LiFePO_4$ films with Ts is shown in Figure 4.13. It can be seen that the electrical conductivity decreases with increasing Ts. Therefore, the conductivity will be decrease if T_s is increasing. The electrical resistivity of pure $LiFePO_4$ is 10^7 Ω-m [40]. The electrical resistivity of RF sputter deposited $LiFePO_4$/C thin film is at the order of 10^2 Ω-m [45]. Our results are in good agreement with these works. The difference in the results it is due to that the films were sputtered from a pure $LiFePO_4$ target without any conducting media such as carbon or metals imbedded [48].

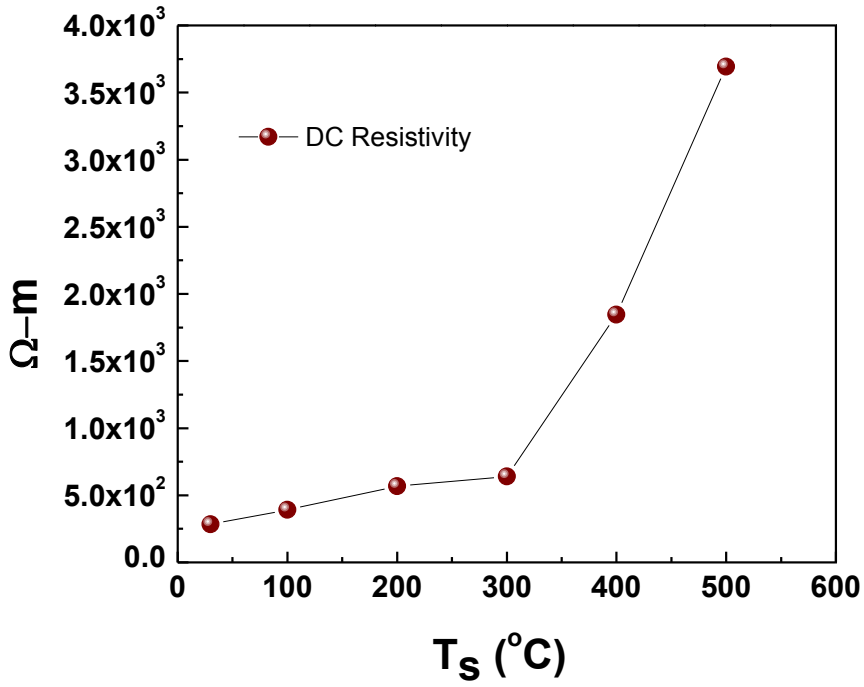

Figure 4.13: Changes of electrical resistivity of $LiFePO_4$ samples with growth temperature

The frequency dependence of the electrical conductivity (σ_{ac}) of $LiFePO_4$ films grown from RT-500 °C is shown in Figure 4.14. The total conductivity of the films can be expressed by the relationship:

$$\sigma_{tot} = \sigma_0(T) + \sigma(\omega, T) \text{--------(3)} \quad (7)$$

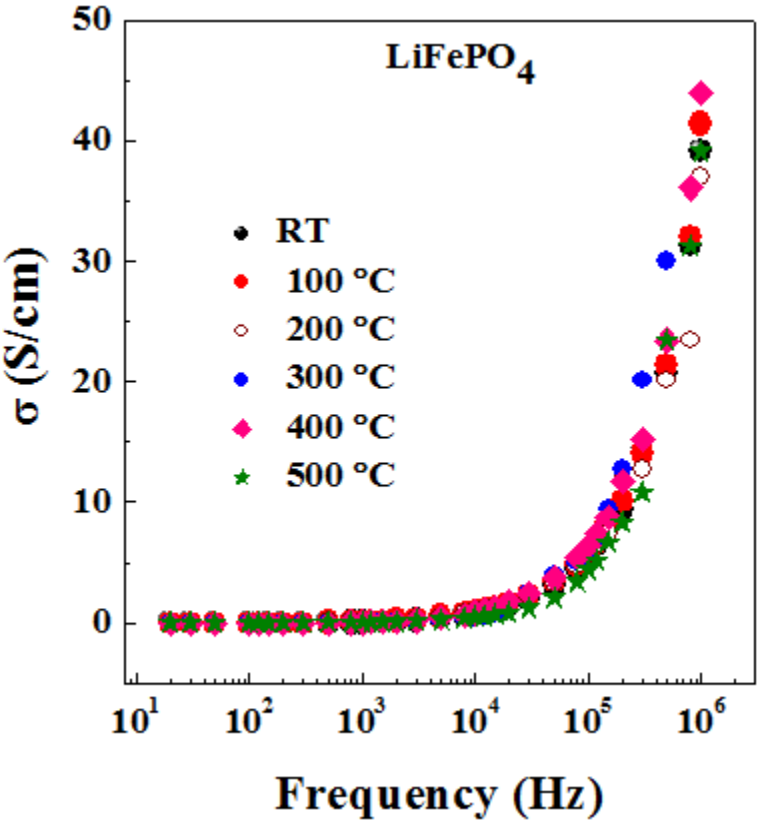

Figure 4.14: Frequency dependence of the electrical conductivity

The first term at R.H.S. is the dc conductivity due to the band conduction, which is frequency independent. On the other hand, second term of the equation is purely a representation of the ac conductivity due to the electron hoping between the Fe^{2+}/Fe^{3+} ions.

$LiFePO_4$ has an ordered olivine structure (space group Pnma). The oxygen atoms are arranged in a slightly distorted, hexagonal close-packed arrangement. The FeO_6 octahedra share

common corners in the bc plane, and the LiO_6 octahedra form an edge-sharing chain in the b-direction. The separation of the FeO_6 octahedra by PO_4 polyanions significantly reduces the electrical conductivity of the material. The electronic conductivity in this material is determined by the mobile electrons in Fe^{2+}/Fe^{3+} redox couple. In addition to that, the hoping mechanism in $LiFePO_4$ films can be attributed to the presence of oxygen vacancies. Based on the $LiFePO_4$ bulk electronic structure, the valence band is formed by the filled O 2*p* orbital and the conduction band is formed by the Metal (Fe) 3*d* orbital. The vacancy level forms below the conduction band and it can also trap one or two electrons. Conductivity increases (by three orders of magnitude) with increasing frequency from 20 Hz to 1 MHz is attributed due to the hoping mechanism in $LiFePO_4$ films.

The observed dispersion in the resistivity is due to the contribution from the O^{2-}, Li^{+} and Fe^{2+}/Fe^{3+} ions to the relaxation. At low frequency regime, hopping of electron between the localized Fe ions increases subsequently the resistivity decreases. The frequency variation of electrical resistivity data was fit to the following equation:

$$\rho - \rho_\infty = \frac{\left(\rho_0 - \rho_\infty\right)}{\left[1 + \left(\omega\tau\right)^{2(1-\alpha)}\right]} --------(4) \qquad \text{.. (8)}$$

Where ρ_∞ is the resistivity value at 1 MHz, ρ_0 is the resistivity value at 20 Hz, τ is the mean relaxation time (3.4, 3.3, 3.1, 2.8, 2.5 and 2.2 μs for the films grown from T_s=RT to 500 ºC) and α is the spreading factor (about the Figure 4.16) mean relaxation time (0.62, 0.60, 0.57, 0.53 and 0.51 for the films grown from T_s=RT to 500 ºC). The calculated mean relaxation time values are found to decrease from 3.4 μs to 2.5 μs with increasing T_s from RT to 500 ºC due to the increase in conductivity. Figure 4.15 shows the variation of the mean relaxation time with increasing T_s. τ is seen to decrease with increasing T_s. Increasing grain size with increasing T_s

subsequently the decreasing grain boundary scattering leads to decreasing resistivity and the mean relaxation time.

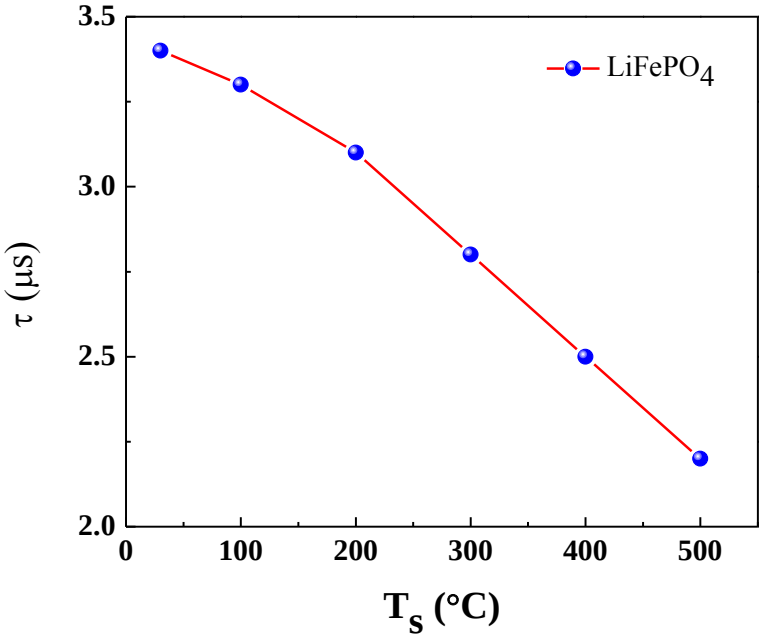

Figure 4.15: Relaxation Time

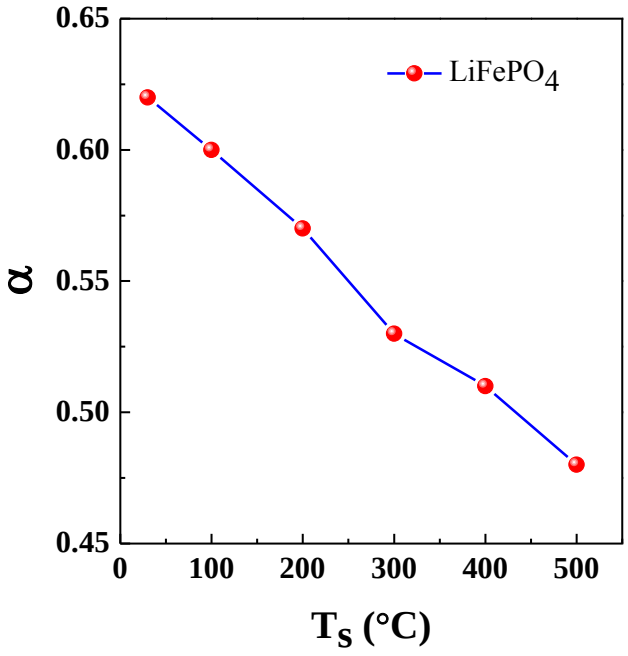

Figure 4.16: Spreading Factor

Chapter 5: Conclusions

$LiFePO_4$ thin films were fabricated using Si wafers (100) and quartz substrates and a RF magnetron sputtering system. The effect of growth temperature (RT-500 °C) and annealing temperature (400-800 °C) on the structure, surface/ interface morphology, chemical quality, and optical and electrical properties of $LiFePO_4$ films was investigated. XRD and HRSEM results indicate that the effect of growth temperature on the $LiFePO_4$ films is significant. Samples grown from RT-500 °C are amorphous while those annealed from 600-800 °C are crystalline. The grain size increase as the temperature is increased. Therefore, it is concluded that the crystal-size can be obtained by carefully controlling the growth temperature. The effect of T_s was significant on the optical characteristics of $LiFePO_4$ films. The microstructure effects were remarkably evident in the optical spectra and band gap analysis. The transmittance of the films decreased with the increase in T_s. The decrease in band gap of $LiFePO_4$ films (2.75-3.75 eV; RT-800 °C) is due to the oxygen vacancies. The highest band gap 3.75 eV was obtained by annealed the sample at 600 °C for 2 hours. The corresponding electrical resistivity of the samples increases with increase in T_s which is due to improvement in the crystal structure. The T_s-E_g and T_a-E_g relationships found for $LiFePO_4$ films suggest that the electronic structure can be tuned by achieving control over the growth temperature or post-deposition annealing conditions. A direct correlation between growth conditions, microstructure and electronic properties as noted in this work is useful to design $LiFePO_4$ thin films for microbattery applications.

Chapter 6: Future Work

The scope for the future work and some directions are as listed below.

1. The $LiFePO_4$ films grown can be tested for electrochemical performance.
2. The optimized conditions from this work can be used to construct a microbattery.
3. Doping with some carbon can be considered to improve its low conductivity.

References

1. Xia Yonggao.; Yoshio Masaki.; Noguchi Hideyuki.; "Improved electrochemical performance of $LiFePO_4$ by increasing its specific surface area." *Electrochimica Acta.* **2006**, 52.
2. Prosini Pier Paolo.; Zane Daniela.; Pasquali Mauro.; "Improved electrochemical performance of a $LiFePO_4$-based composite cathode" *Electrochimica Acta.* **2001**, 46, 3517.
3. Zhi Xiaoke.; Liang Guangchuan.; Wang Li.; Ou Xiuqin.; Zhang Jingpeng.; Cui Junyan.; "The cycling performance of $LiFePO_4$/C cathode materials." . *Journal of Power Sources.* **2009**,189,779.
4. Mauger A.; Gendron F.; Julien C.M.; "Magnetic properties of lithium intercalation compounds." *Ionics*. **2006**, 21–32.
5. Chiu K.F.; Chen C.L.; **"**Electrochemical performance of magnetron sputter deposited $LiFePO_4$-Ag composite thin film cathodes." *Surface & Coatings Technology*. **2010**.
6. Takahashi Masaya.; Tobishima Shinichi.; Takei Koji.; Sakurai Yoji.; "Characterization of $LiFePO_4$ as the cathode material for rechargeable lithium batteries." *Journal of Power Source*s. **2001**, 97, 508.
7. Liu Xu-heng.; Zhao Zhong-wei.; "Synthesis of $LiFePO_4$/C by solid–liquid reaction milling method." *Powder Technology*. **2010**, 197, 309.
8. Marcella Bini.; Maria Cristina Mozzati.; PietroGalinetto.; Doretta Capsoni.; Stefania Ferrari.; Marco S.Grandi.; Vincenzo Massarotti.; "Structural, spectroscopic and magnetic investigation of the $LiFe_{1-x}Mn_xPO_4$ (x=0–0.18) solid solution." *J. Solid State chem.* **2009**, 1972-1981.

9. Liu Youyong.; Cao Chuanbao.; Li Jing.; "Enhanced electrochemical performance of carbon nanospheres–$LiFePO_4$ composite by PEG based sol–gel synthesis." *Electrochimica Acta*. **2010**, 55, 3921.
10. Ramana C.V.; Mauger A .;, Gendron F .; Julien C.M.; Zaghib K .; "Study of the Li-insertion/extraction process in $LiFePO_4/FePO_4$." *Journal of Power Sources*. **2009**, 187, 555.
11. Li Jianling.; Suzuki Tomohiro.; Naga Kazuhisa.; Ohzawa Yoshimi.; Nakajima Tsuyoshi.; "Electrochemical performance of $LiFePO_4$ modified by pressure-pulsed chemical vapor infiltration in lithium-ion batteries." *Materials Science and Engineering.* **2007**, 142, 86.
12. Santoro R.P.; Newnhma R.E.; "Antiferromagnetism in $LiFePO_4$*." Acta Cryst*. **1967**, 22-344.
13. Zaghib K.; Mauger A.; Goodenough J.B.; Gendron F.; Julien M.; "Electronic, Optical, and Magnetic Properties of $LiFePO_4$: Small Magnetic Polaron Effects*." Chem. Mater.* **2007**, 19.
14. Yamada A.; Chung S.C.; Hinokuma K.; "Optimized $LiFePO_4$ for lithium battery cathodes*." J. Electrochem. Soc.* **2001**, 148, A224.
15. Padhi A.K.; Nanjundaswamy K.S.; Goodenough J. B.; "Phospho-olivines as Positive-Electrode Materials for Rechargeable Lithium Batteries." *J. Electrochemical. Society*.**1997**, 144, 1609.
16. Ravet N.; Goodenough J.B.; Besner S.; Simoneau M.; Hovington P.; Abstract 127.*The Electrochemical Society and The Electrochemical Society of Japan Meeting Abstracts*. **1999**, 99.

17. Ait-Salah.J A.; Dodd, A. Mauger.; Yazami R.; F. Gendron.; Julien C.M.; "Structural and Magnetic Properties of $LiFePO_4$ and Lithium Extraction Effects*." DOI*: 10.1002. **2006.**

18. Arcon Denis.; Zorko Andrej.; Dominko Robert.; Jagli Zvonko.; "A comparative study of magnetic properties of $LiFePO_4$ and $LiMnPO_4$." *JOURNAL OF PHYSICS: CONDENSED MATTER*. **2004**, 16.

19. Kim Woo.; Cheol.; Tae Jeong Woon .; Sub Lee Kyung.; "Synthesis and electrochemical properties of olivine $LiFePO_4$ as a cathode material prepared by mechanical alloying." *Journal of Power Sources*. **2004**, 137, 93.

20. Bini Marcella.; Mozzati Maria Cristina.; Galinetto Piestro.; Capsoni Doretta.; Ferrari Stefania.; Grandi Marco S.; Massarotti Vicenzo.; "Structural, spectroscopic and magnetic investigation of the $LiFe_{1-x}Mn_xPO_4$ (x=0–0.18) solid solution." *Journal of Solid State Chemistry*. **2009**, 189.

21. M. Kope M.; Yamada A.; Kobayashi G.; Nishimura S.; Kanno R.; Mauger A.; Gendron F.; Julien C.M.; "Structural and magnetic properties of $Li_x(Mn_yFe_{1-y})PO_4$ electrode materials for Li-ion batteries." *Journal of Power Sources*. **2009**, 189.

22. Wang G.X.; Needham S.; Yao J.; Wan J.Z.; Liu R.S.; Liu H.K.; "A study on $LiFePO_4$ and its doped derivatives as cathode materials for lithium-ion batteries." *Journal of Power Sources*. **2006**, 159.

23. Sang Jun Kwon .; Myung Seung-Taek.; Komaba Shinichi.; Hirosaki Norimitsu.; Yashiro Hitoshi.; Kumagai Naoaki.; "Emulsion drying synthesis of olivine $LiFePO_4$/C composite and its electrochemical properties as lithium intercalation material." *Electrochimica Acta*. 2004, 49.

24. Kuwahara Akira.; Suzuki Shinya.; Miyayama Masaru.; "High-rate properties of $LiFePO_4$/carbon composites as cathode materials for lithium-ion batteries." *Ceramics* International. **2008**, 34.
25. Ritchie Andrew.; Howard Wiltmon.; "Recent developments and likely advances in lithium-ion batteries." *Journal of Power Sources*. **2006**, 162.
26. Patro Laxmi Narayana.; Hariharan K.; "Frequency dependent conduction characteristics of mechanochemically synthesized $NaSn_2F_5$." *Materials Science and Engineering.* **2009**, 173.
27. Patro Laxmi Narayana.; Hariharan K.; "AC conductivity and scaling studies of polycrystalline SnF_2." *Materials Chemistry and Physics*. **2009**, 116.
28. Denis Arcon.; Andrej Zorko.; Robert Dominko.; "A comparative study of magnetic properties of $LiFePO_4$ and $LiMnPO_4$." *Journal of Physics: Condensed Matter*. **2004**, 5531–5548.
29. Ravet N.; Gauthier M.; Zaghib K.; Goodenough J.B.; Mauger A.; Gendron F.; Julien C.M.; "Mechanism of the Fe^{+3} Reduction at Low Temperature for $LiFePO_4$ Synthesis from a Polymeric Additive." *Chem. Matter*. **2007,** 2595-2602.
30. Ait-Salah A.; Dodd J.; Mauger A.; Yazami R.; Gendron F.; Julien C.M.; "Structural and Magnetic Properties of $LiFePO_4$ and Lithium Extraction Effects. Z. Anorg." *Allg. Chem*. **2006**, 1598-1605.
31. Zaghib K.; Mauger A.; Gendron F.; Julien C.M.; "Surface Effects on the Physical and Electrochemical Properties of Thin LiFePO4 Particles." *Chem. Mater*. **2008**, 462–469.

32. Hannoyer B.; Prince M.; Jean M.; Liu R.S.; Wang G.X.; "Mössbauer study on $LiFePO_4$ cathode material for lithium ion batteries." *Springer Science and Business Media B.V.* **2006**.

33. Creer J.G.; Troup G.J.; "The magnetic susceptibility of $LiFePO_4$ and $LiCoPO_4$." *Physics Letters A.* **1970**, 439-440.

34. Zhou Fei.; Kang Kisuk.; Maxisch Thomas.; Ceder Gerbrand.; Morgan Dane**.; "**The electronic structure and band gap of $LiFePO_4$ and $LiMnPO_4$." *Solid State Communications*. **2004**, 181–186.

35. Li Zhihua.; Zhang Duanming.; Yang Fengxia.; "Developments of lithium-ion batteries and challenges of $LiFePO_4$ as one promising cathode material." *J Mater Science*. **2009**, 44:2435–2443.

36. Byoungwoo Kang.; Gerbrand Cede.; "Battery materials for ultrafast charging and discharging." *Nature.* **2009**, 190-193.

37. Gullapalli, S. K.; Vemuri, R. S.; Manciu, F. S.; Enriquez, J. L.; Ramana, C. V.; "Tungsten oxide WO_3 thin films for application in advanced energy systems." *Journal of vacuum Science Technolog A.* **2010**, 28, 824.

38. Gullapalli, S. K.; Vemuri, R. S.; Ramana, C. V.; "Structural transformation induced changes in the optical properties of nanocrystalline tungsten oxide thin films." *Applied Physics Letters.* **2010**, 96, 171903.

39. Xian-Jun Zhu.; Long-Bin Cheng.; Cheng-Gang Wang.; Zai-Ping Guo.; Peng Zhang.; Guo-Dong Du.; Hua-Kun Liu.; "Preparation and Characteristics of $LiFePO_4$ Thin Film by Radio Frequency Magnetron Sputtering for Lithium Microbatteries" *J. Phys. Chem. C.* **2009**, 14518–14522.

40. Iltchev Nick.; Chen Yike.; Okada Shigeto.; Yamaki Jun-ichi .; **"**$LiFePO_4$ storage at room and elevated temperatures." *Journal of Power Sources*. **2003**, 119-121.
41. Yang Shoufeng.; Song Yanning.; Ngala Katana.; Zavalij Peter Y.; Whittingham M. Stanley.; **"**Performance of $LiFePO_4$ as lithium battery cathode and comparison with manganese and vanadium oxides." *Journal of Power Sources*. **2003**, 239–246.
42. M. Zhao, S. Kariuki, H. D. Dewald, F. R. Lemke, R. J. Staniewicz, E. J. Plichta and R. A. Marsh, *J. Electrochem. Soc.* **2000**, 147, 2874.
43. M. M. Thackeray, A. Kock, M. H. Rossouw, D. Liles, R. Bittihn and D. Hoge, *J. Electrochem. Soc.* 1992, 139-363.
44. J. W. Braithwaite, A. Gonzales, G. Nagasubramanian, S. J. Lucero, D. E. Peebles, J. A. Ohlhausen and W. R. Cieslak, *J. Electrochem. Soc.* **1999**, 146-448.
45. Xian-Jun Zhu.; Long-Bin Cheng.; Cheng-Gang Wang.; Zai-Ping Guo.; Peng Zhang.; Guo-Dong Du.; Hua-Kun Liu.; "Preparation and Characteristics of $LiFePO_4$ Thin Film by Radio Frequency Magnetron Sputtering for Lithium Microbatteries." *J. Phys. Chem. C.* **2009**, 14518–14522.
46. Chiu K.F.; Chen P.Y.; "Structural evolution and electrochemical performance of $LiFePO_4$/C thin films deposited by ionized magnetron sputtering." Surface & Coatings Technology. **2008**, 872–875.
47. Xie J.; Imanishi N.; Zhang T.; Hirano A.; Takeda Y.; Yamamoto O.; "Li-ion diffusion kinetics in $LiFePO_4$ thin film prepared by radio frequency magnetron sputtering." *Electrochimica Acta.* **2009**, 4631–4637.
48. Sauvage F.; Baudrin E.; Gengembre L.; Tarascon J.M.; "Effect of texture on the electrochemical properties of $LiFePO_4$ thin films." *Solid State Ionics.* **2005**, 1869–1876.

49. Kun Tang.; Jinpeng Sun.; Xiqian Yu.; Hong Li.; Xuejie Huang.; "Electrochemical performance of $LiFePO_4$ thin films with different morphology and crystallinity." *Electrochimica Acta*. **2009**, 6565–6569.
50. Subrahmanyam, A.; Karuppasamy, A.; "Optical and electrochromic properties of oxygen sputtered tungsten oxide (WO_3) thin films." *Sol. Energy Mater. Sol. Cells.* 2007, 91, 266.
51. Tepehan, F. Z.; Ghodsi, F. E.; Ozer, N.; Tepehan, G. G.; "Optical properties of sol-gel dip-coated Ta_2O_5 films for electrochromic applications." *Sol. Energy Mater. Sol. Cells.* 1999, 59, 265.
52. Ruhul Amin.; Palani Balaya.; Joachim Maier.; "Anisotropy of Electronic and Ionic Transport in $LiFePO_4$ Single Crystals." Electrochem. Solid-State Letters. **2007**, A13-A16.
53. Washizu, E.; Yamamoto, A.; Abe, Y.; Kawamura, M.; Sasaki, K.; "Optical and electrochromic properties of RF reactively sputtered WO_3 films." *Solid State Ionics*. 2003, 165, 175.
54. M. Saiful Islam.; Daniel J. Driscoll.; Craig A. J. Fisher.; Peter R. Slater.; "Atomic-Scale Investigation of Defects, Dopants, and Lithium Transport in the $LiFePO_4$ Olivine-Type Battery Materia;." *Chem. Mater.* **2005**, 5085–5092.
55. Tyagi, P.; Vedeshwar, A. G.; "Effect of residual stress on the optical properties of CdI_2 films." Phys. Rev. B. **2002**, 66, 075422.
56. Goldstein, J.; Newbury, D.; Joy, D.; Lyman, C.; Echlin, P.; Lifshin, E.; Sawyer, L.; Michael, J.; "Scanning Electron Microscopy and X-ray Microanalysis." *Kluwer Academic/Plenum*, New York, **2003**.

57. Goldstein, J.; Newbury, D.; Joy, D.; Lyman, C.; Echlin, P.; Lifshin, E.; Sawyer, L.;Michael, J.; "Scanning Electron Microscopy and X-ray Microanalysis." *Kluwer Academic/Plenum*, New York, **2003**.

58. Ramana, C. V.; Ait-Salah, A.; Utsunomiya, S.; Becker, U.; Mauger, A.; Gendron, F.; Julien, C. M.; "Structural Characteristics of Lithium Nickel Phosphate Studied Using Analytical Electron Microscopy and Raman Spectroscopy." *Chem. Mater.* **2006**, 18, 3788.

59. Ramana, C. V.; Smith, R. J.; Julien, C. M.; "Growth and surface characterization of V_2O_5 thin films made by pulsed-laser deposition." *J. Vac. Sci. Technol. A.* **2004**, 22, 2453.

60. Liming Feng.; Teng Gai.; Xue Wei.; " Influence of Nanotubes on the Performance of $LiFePO_4$." *Advanced Materials Research*. **2011**, 148-149.

Curriculum Vita

Jose Marcos Mares was born on February 9th, 1984 in Cd. Juarez, Chihuahua, Mexico. The last son of Leonor Gonzalez and Jose Mares, he graduated from the University of Texas at El Paso with a Bachelor of Science in Mechanical Engineering in Fall 2008. During that time, he was working as a peer leader for pre-calculus and calculus classes. Then he started to pursue his master's degree at the same University in Mechanical Engineering. While pursuing a master's degree, he worked as a teaching assistant and research assistant in the department of mechanical engineering. In Fall 2010, he graduated with a Master of Science degree in Mechanical Engineering and proceeded to work as a mechanical engineer in the Mexican Automotive Industry.

Permanent Address: 229 Morning Dawn Avenue

El Paso, Texas 79932